

VELOCITY MODIFICATION OF HI POWER SPECTRUM

A. LAZARIAN^{1,2,3} D. POGOSYAN²

The distribution of atomic hydrogen in the Galactic plane is usually mapped using the Doppler shift of 21 cm emission line and this causes the modification of the observed emission spectrum. We calculate the emission spectrum in velocity slices of data (channel maps) and derive its dependence on the statistics of velocity and density fields. We find that (a) if the density spectrum is steep, i.e. $n < -3$, the short-wave asymptotics of the emissivity spectrum is dominated by the velocity fluctuations; (b) the velocity fluctuations make the emission spectra shallower, provided that the data slices are sufficiently thin. In other words, turbulent velocity creates small scale structure that can erroneously be identified as clouds. The effect of thermal velocity is very similar to the change of the effective slice thickness, but the difference is that while an increase of the slice thickness increases the amplitude of the signal the increase of the thermal velocity leaves the measured intensities intact while washing out fluctuations. The contribution of fluctuations in warm HI is suppressed relative to cold component when velocity channels used are narrower than warm HI thermal velocity and small angular scale fluctuations are measured. We calculate how the spectra vary with the change of velocity slice thickness and show that the observational 21 cm data is consistent with the explanation that the intensity fluctuations within individual channel maps are generated by a turbulent velocity field. As the thickness of velocity slices increases density fluctuations get to dominate emissivity. This allows to disentangle velocity and density statistics. The application of our technique to the Galactic and SMC data reveals spectra of density and velocity with the power law index close to $-11/3$. This is a Kolmogorov index, but the explanation of the spectrum appealing to the Kolmogorov-type cascade faces substantial difficulties. We generalize our treatment for the case of a statistical study of turbulence inside individual clouds. The mathematical machinery developed is applicable to other emission lines.

Subject headings: interstellar medium: general, structure-turbulence-radio lines; atomic hydrogen

1. INTRODUCTION

Galactic HI is an important component of the interstellar media (McKee & Ostriker 1977) and much efforts have been devoted to its studies (see Burton 1992). In particular, Crovisier & Dickey (1983) and Green (1993) measured the spectrum of 21 cm intensity fluctuations in order to get a handle on the statistical properties of this media. Lazarian (1995, henceforth L95) suggested a statistical inversion technique for HI interferometric data (see also Lazarian 1994 a,b). Note that statistical description is a nearly indispensable strategy while dealing with turbulence⁴. Indeterminism of turbulence implies that two virtually identical systems develop very different patterns of turbulent motions. The advantage of statistical techniques is that they extract underlying regularities of the flow and reject incidental details.

Attempts to study interstellar turbulence date as far back as 50s (Horner 1951, Munch 1958, Wilson et al. 1959) and various directions of research achieved various degree of success (see reviews by Kaplan & Pickelner 1970, Dickman 1985, Lazarian 1992, Armstrong, Rickett & Spangler 1995). Studies of turbulence statistics of ionized media were successful (see Spangler & Gwinn 1990, Narayan 1992) and provided the information of the statistics of plasma density⁵ at scales 10^8 - 10^{15} cm. This research profited

¹Department of Astrophysical Sciences, Princeton University, Princeton

²Canadian Institute for Theoretical Astrophysics, University of Toronto

³Present address: Dept. of Astronomy, University of Wisconsin, Madison

⁴Speaking about interstellar turbulence we understand it in terms of unpredictable spatio-temporal behavior of nonlinear systems (Scalo 1985, 1987) and accept that Kolmogorov picture may be too simplistic while dealing with such complex media (Lazarian 1999).

⁵Incidentally the found spectrum was Kolmogorov one.

a lot from clear understanding of processes of scintillations and scattering achieved by theorists (see Goodman & Narayan 1985, Narayan & Goodman 1989).

Deficiencies in the theoretical description have been, to our mind, the major impediments to studies of turbulence in the neutral part of the interstellar medium. For instance, important statistical studies of molecular clouds (Dickman & Kleiner 1985, Miesch & Bally 1994) has not achieved the success parallel to the one in scintillation studies. These problems were addressed in L95, where the quantitative study of deconvolution of the 3D statistics from the data averaged along the lines of sight was presented (see also Lazarian 1999a).

However, the issue of velocity distortions of the observed spectrum was treated only qualitatively in L95, and this motivates our present study. Indeed, even in the absence of density fluctuations in Galactic coordinates velocity fluctuations would make the distribution of emission inhomogeneous in velocity data cubes. The release of the Canadian Galactic Plane survey data makes this work very timely.

The present paper concentrates on the studies of HI in Galactic plane. It also addresses the issue of studies of individual clouds. We deliberately restrict our attention to HI, although the presented technique is potentially applicable to other spectral lines. The pervasive distribution of neutral hydrogen presents a sharp contrast to the localized distribution of molecular species and this alleviates problems with averaging⁶ (cf. Houligan & Scalo 1990). The remarkable constancy of the slope of the intensity power spectrum measured by Green (1993) and Stanimirovic et al (1998) indicates that the HI sample is homogeneous in a statistical sense. However, most of our results are applicable to other emission lines.

It may seem that the Galactic plane presents simultaneously the best and the worst case for obtaining HI statistics. On one side, the Galactic rotation curve presents a natural distance indicator, which allows to roughly segregate emission from different parts of Galactic disk. On the other side, the random velocity is being confused with the one arising from regular rotation resulting in distance errors.

To what extent the statistics of the underlying density can be recovered is the issue this paper deals with. The effects of projection and velocity distortions plague the statistical studies of turbulence in interstellar clouds. This paper provides a guide on how to deal with such problems. We aimed our paper at providing a general mathematical formalism necessary for dealing with velocity distortions of the observed intensity fluctuations. Modifications of the technique and its application to various emission/absorption lines will be done elsewhere.

Another motivation for our study stems from recent attempts to describe the structures in the Galactic hydrogen in order to estimate the fluctuations of microwave polarization arising from interstellar dust. This contribution is extremely important in view of present-day efforts in the CMB research (see Prunet & Lazarian 1999, Draine & Lazarian 1999). Some of the studies, for instance, one by Sethi, Prunet and Bouchet (1998) attempts to relate the statistics of density observed in the velocity space and the statistics of magnetic field fluctuations. Our present work and a subsequent paper show that the relation between the two statistics is far from trivial and velocity fluctuations may create a lot of emissivity structures in the channel maps.

The distortion of the density statistics in the presence of velocity fluctuations is important for understanding of the large-scale distribution of galaxies. The corresponding literature is vast and we just mention a pioneering study by Kaiser (1987) and a recent review by Hamilton (1998). In cosmology the problem is known as the problem of 'redshift-space' corrections to the statistics of galaxy distribution and has been addressed predominantly under the linear regime of the gravitational instability or at the regime when the velocity contribution to the Fourier spectrum can be factorized, e.g. by a Maxwellian factor (see Hamilton (1998)). The problem that we study is much richer. We have to deal with the case of general, nonlinear, density fields transformed by coherent turbulent velocities. Development of the formalism for HI studies requires to consider a variety of spectra, including steep (e.g. Kolmogorov) power spectra which have never been addressed in cosmological literature.

Our treatment of the problem is based on the description of HI statistics in terms of power spectra.

⁶ A study by Stutzki et al (1998) shows that the worries about the turbulence homogeneity are probably exaggerated even in the case of molecular clouds. At least the wavelet analysis that they used revealed a well-defined spectrum of turbulence.

Such a description is traditional in hydrodynamics and MHD theory and it allows to relate the statistics of interstellar media to the statistics of idealized fluids. Moreover, spectra provide a useful intuitive insight to the properties of turbulence. For instance, shallow spectra correspond to more structure at a small scale, while steep spectra correspond to a random field dominated by large-scale fluctuations. Other descriptors are reviewed in Lazarian (1999b).

An additional complication arises from variations of gas temperature. Gas thermal velocity smears up the turbulent velocity effects and this smearing effect depends on the temperature. In the paper we show that in most circumstances the intensity fluctuations are due to cold HI.

In what follows, we formulate the problem of velocity mapping, discuss the 3D power spectrum of intensity that can be measured in velocity data cubes (section 2). Then we show how the 2D spectra of channel maps (those spectra can be directly obtained using an interferometer) depend on the thickness of the velocity slice (section 3). For power-law density and velocity statistics we calculate analytically and numerically the 2D spectra when the density is dominated by small-scale and large-scale inhomogeneities (section 4). We compare our predictions with the available Galactic and Small Magellanic Cloud (SMC) observational data in section 5, while section 6 contains a qualitative discussion of our results and presents an outline of the outstanding problems. We provide the summary of our results in section 7. To simplify our presentation we moved derivation of many results into Appendixes. They, however, have the value on their own. For instance, Appendix B presents asymptotics of 3D spectra in velocity space, while Appendix C contains derivations for correlation functions in velocity space. The modification of our analysis when velocity and density fields are correlated is presented in Appendix D. Appendix E describes a statistical treatment of emission from individual HI clouds and establishes the connection between this treatment and the treatment of fluctuations of intensity from HI Galactic disc that the main body of the paper deals with. Note, that it is this modification of the technique that is most important for studying turbulence in molecular clouds. Appendix F describes additional statistical tools, namely, 1D radial spectra which can be useful measures of density and velocity.

2. THE PROBLEM.

2.1. *The Model.*

In studying Galactic HI observers use a model Galactic rotation curve (see Kerr et al 1986) to identify points along the line of sight in their data cubes, in which one of the coordinates is the Doppler shifted velocity. The model curves reflect the averaged motion of HI in the Galactic potential or bulk deviations from circular motions and therefore are accurate up to turbulent velocities.

It is easy to understand that the random velocity field makes statistics of emissivity different from the statistics of density. Indeed, the velocity fluctuations can make two emitting elements at different distances from the observer to overlap in the velocity space producing an element of doubled emissivity.

In the present paper we address an important issue of relating the the spectrum of HI emissivity in *velocity* space xyv (v is the z -component of velocity⁷ to density fluctuations in real space xyz coordinates, where z is directed along the line of sight and x & y span the sky plane. The statistics in xyz coordinates is essential for understanding HI structure and processes of fragmentation (see Scalo 1985), while observations provide us with the statistics of velocity data cubes.

Although the problem of relating statistics in velocity space and Galactic coordinates is quite general, in what follows, we limit ourselves to the case of 21 cm emission. HI observations include high precision measurements of Doppler shifted emission lines. For the sake of simplicity, further on we shall disregard self-absorption of the emitted radiation. This looks as a reasonable assumption as numerous studies (see Braun 1997, 1999, Higgs 1999) confirm that for many HI regions self-absorption is negligible⁸.

2.2. *Space-Velocity Mapping.*

⁷These coordinates are also called PPV coordinates which abbreviates Position-Position-Velocity (see Vazquez-Semadeni 1999).

⁸In general, if absorption is localized in the form of individual blobs of dense cold material, those only alter marginally statistical measures on the sizes less than the size of blobs (L95).

The data of HI surveys is stored as data cubes with velocity $v = |\vec{v}_z|$ constituting the third, z , dimension. We analyze what effect the mapping from the xyz space to the xyv space has on the power spectrum of HI density. First, HI gas experience the regular motion induced by galactic rotation. A model of Galactic rotation provides a relation between the z projection (the only projection available through Doppler measurements) of regular velocity v_z^{reg} and the distance along the line of sight, i.e. $v_z^{reg} = \phi(\mathbf{x})$. If observations are made in the slices of the finite thickness the function ϕ can be expanded into Taylor series around a particular point (e.g. the center of data slice with $v_{z0}^{reg} = \phi(z_0)$), $v_z^{reg} = \phi(\mathbf{x}_0) + \phi_{,\mathbf{x}}(\mathbf{x}_0)(\mathbf{x} - \mathbf{x}_0) + 1/2\phi_{,\mathbf{x},\mathbf{x}'}(\mathbf{z}_0)(\mathbf{x} - \mathbf{x}_0)(\mathbf{x}' - \mathbf{x}_0) + \dots$

In addition to the regular part \mathbf{v}^{reg} arising from Galactic rotation the total observed velocity of a gas element \mathbf{v}^{obs} , also contains a random, turbulent, part \mathbf{u} , so that $\mathbf{v}^{obs} = \mathbf{v}^{reg} + \mathbf{u}$. Therefore the mapping from velocity space to Galactic coordinates becomes more involved. Most interesting effects on HI statistics in velocity space arise from the random \mathbf{u} part. We simplify their treatment by approximating the regular z -component of velocity by the linear, z only dependent term:

$$z_s = z_{s0} + A [\phi_{,z}(z_0)(z - z_0) + u_z] \quad (1)$$

where z_s is velocity coordinate in spectral-line data cubes, A is an arbitrary scaling coefficient that relates velocity and data cube length units. Naturally, a linear mapping given by eq. (1) is only correct if the nonlinear terms in the expansion of ϕ are small (in other words, we consider the region of space where coherent flow can be described as flow of a constant shear) and the scales of interest in image plane are sufficiently short that x, y dependence of the shear can be ignored⁹.

To describe turbulence in Galactic disc we find advantageous to use parameter $f(z_0) = \phi_{,z}(z_0)^{-1}$ and put $A = f$. Using vector notations we describe the effect of a random velocity \mathbf{u} as a *linear* map from Galactic frame \mathbf{x} to the velocity-space coordinates \mathbf{x}_s

$$\mathbf{x}_s = \mathbf{x} - f(\mathbf{x}_0) (\mathbf{u} \cdot \hat{\mathbf{z}}) \hat{\mathbf{z}} \quad , \quad (2)$$

Here $\hat{\mathbf{z}}$ is a unit vector along the line of sight, \mathbf{x} is the actual Galactic coordinate of the emitting HI element and \mathbf{x}_s is the position calculated using the Galactic rotation curve (see Blitz & Spergel 1991). We shall note that the values of f vary from slice to slice in accordance with the Galactic rotation curve. In our Galaxy f is of order of 100 pc/(km/s), although it depends on the direction and depth of observations.

A limiting case of the mapping corresponds to the study of individual HI clouds. We discuss this case in Appendix E and present a generalized form of the map applicable for the zero shear, i.e. $f^{-1} \rightarrow 0$.

2.3. Spectrum in the Velocity Space

The relevant expression for the spectrum of density *in velocity space* has been derived by Scoccimarro, Couchman & Frieman (1999). Let us write the Fourier component of the density $\rho(\mathbf{x}_s)$ in velocity space as the sum over positions \mathbf{x}_s^a of all hydrogen atoms

$$\rho_s(\mathbf{k}) = \sum_{atoms} e^{i\mathbf{k} \cdot \mathbf{x}_s^a} = \sum_{atoms} e^{i[\mathbf{k} \cdot \mathbf{x}^a - f(\mathbf{k} \cdot \hat{\mathbf{z}})(\mathbf{u}^a \cdot \hat{\mathbf{z}})]} \quad , \quad (3)$$

In a coarse-grained fluid description of HI atom density in real space, the summation over all atoms is replaced by a continuous integral in the xyz (real space) coordinates: $\sum_{atoms} \Rightarrow \int d^3\mathbf{x} \rho(\mathbf{x})$ with gas density $\rho(\mathbf{x})$. Velocities of individual atoms are averaged¹⁰ over the thermal distribution $\langle \exp[-if(\mathbf{k} \cdot$

⁹It is obvious that if the velocity of Galactic rotation is V_{max} then $\phi_{,zz}(z_0)(z - z_0)/\phi_{,z}(z_0) \sim (\delta V/V_{max})$, where δV is equal or less than the thickness of a velocity slice. For sufficiently small slice thickness the factor $(\delta V/V_{max})$ is small and the contribution of the nonlinear term is negligible. It will be clear from the discussion below that studying turbulence at a particular scale one should account for the non-linearity of ϕ on this scale. Similarly, fluctuations are observed over a limited area of $\delta x \delta y$ plane and one can use $\phi(z_0, x_0, y_0)$ to characterize the regular velocity if variations of ϕ on the distances studied are small. This variation decreases with a distance to the slice. It is easy to see that this requirements for the map to be linear are easy to fulfill.

¹⁰The averaging is similar to that presented by eq. (10).

$\hat{\mathbf{z}})(\mathbf{u}^a \cdot \hat{\mathbf{z}})]_{thermal} = \exp[-ifk_z u_z(\mathbf{x})] \exp[-f^2 k_z^2 v_T^2 / 2]$, where $\mathbf{u}(\mathbf{x})$ is now the peculiar turbulent velocity of the fluid element at position \mathbf{x} . Thermal velocity with one dimensional mean-square $v_T = 0.75 \left(\frac{T}{100\text{K}}\right)^{1/2}$ km/s is incoherent and acts as a smoothing along the velocity coordinate, limiting the resolution in velocity space. Thus we obtain for density Fourier amplitude

$$\rho_s(\mathbf{k}) = e^{-f^2 k_z^2 v_T^2 / 2} \int d^3 \mathbf{x} \rho(\mathbf{x}) e^{-ifk_z u_z(\mathbf{x})} e^{i\mathbf{k} \cdot \mathbf{x}} \quad . \quad (4)$$

The variance of Fourier amplitudes in velocity space is

$$\langle \rho_s(\mathbf{k}) \rho_s^*(\mathbf{k}') \rangle = e^{-f^2 (k_z^2 + k_z'^2) v_T^2 / 2} \int d^3 \mathbf{x} \int d^3 \mathbf{x}' e^{i\mathbf{k} \cdot \mathbf{x} - \mathbf{k}' \cdot \mathbf{x}'} \langle \rho(\mathbf{x}) \rho(\mathbf{x}') e^{-if[k_z u_z(\mathbf{x}) - k_z' u_z(\mathbf{x}')]} \rangle \quad . \quad (5)$$

Henceforth we use angular brackets $\langle \dots \rangle$ to denote ensemble averaging over turbulence realizations. We assume statistical homogeneity of the ensemble in the Galactic frame, i.e. we assume that the average of any expression with two spatial coordinates depends only on the vector separation between these two points. The density Fourier modes in velocity space are then uncorrelated and can be described by the power spectrum¹¹ $P_s(\mathbf{k})$

$$\langle \rho_s(\mathbf{k}) \rho_s^*(\mathbf{k}') \rangle = P_s(\mathbf{k}) \delta(\mathbf{k} - \mathbf{k}') e^{-f^2 k_z^2 v_T^2} \quad (6)$$

$$P_s(\mathbf{k}) = \int d^3 \mathbf{r} e^{i\mathbf{k} \cdot \mathbf{r}} \Xi(\mathbf{k}, \mathbf{r}), \quad \mathbf{r} = \mathbf{x} - \mathbf{x}' \quad , \quad (7)$$

where the kernel is

$$\Xi(\mathbf{k}, \mathbf{r}) = \langle e^{ifk_z (u_z(\mathbf{x}) - u_z(\mathbf{x}'))} \rho(\mathbf{x}) \rho(\mathbf{x}') \rangle \quad . \quad (8)$$

Looking at eq. (8) one easily notices that although both velocity and density contribute to $P_s(\mathbf{k})$ their functional dependences are different. This opens a perspective of separating the velocity and density contributions to the emissivity statistics that we explore in sections 4 and 5.

Eq. (5) assumes a plane-parallel approximation when one does not distinguish between the radial nature of the line of sight and the Cartesian z -direction. The formula is accurate when the HI region is observed from a distance that is large compared to its thickness \mathcal{L}_{sl} . The statistical analysis when the converging geometry of the lines of sight is accounted for is more involved (see Lazarian 1994b) and will be discussed elsewhere.

In what follows we limit ourselves with the discussion of basics of the space-velocity mapping and the role of coherent turbulent velocity. It is easy to see that the thermal velocity effect in z_s direction is similar to the effect of the finite velocity resolution of the telescope in the x and y directions (see L95). To make our formulae more comprehensible we defined the spectrum $P_s(\mathbf{k})$ to contain only correlated turbulent contribution while keeping thermal velocity factor separately. We can neglect thermal effect altogether if we study supersonic turbulence in velocity slices $\delta V > v_T$. We, however, will remember about the high k_z truncation of our spectrum by thermal motions when necessary (see Chapter 3).

To proceed at this stage we make the following assumptions about the properties of the random fields $\rho(\mathbf{x})$ and $\mathbf{u}(\mathbf{x})$. First of all, we assume that the turbulent velocity is uncorrelated with the density in Galactic coordinates, and therefore $\langle e^{if \dots} \rho(\mathbf{x}) \rho(\mathbf{x}') \rangle = \langle e^{if \dots} \rangle \xi(\mathbf{r})$, where the density correlation function is assumed to be isotropic in xyz -space

$$\xi(r) = \xi(\mathbf{r}) = \langle \rho(\mathbf{x}) \rho(\mathbf{x} + \mathbf{r}) \rangle \quad . \quad (9)$$

We discuss the corrections due to velocity-density correlations in Appendix D and show that they are of limited importance for Lognormal model of density fluctuations. Future research will test our assumption for the distributions produced by numerical simulations. Interstellar velocity and density fields can be anisotropic and we discuss this in sections 6.2 and 6.3.

¹¹Here we deal with small scale coherent structures and do not deal with the large scale ones, e.g. spiral arms.

We do not have to make any further assumptions about density statistics. The turbulent velocity we assume to be Gaussian, then

$$\langle e^{if\cdots} \rangle = \int dy \exp(ify) \exp\left(-\frac{y^2}{2\langle\Delta u_i\Delta u_j\rangle\hat{z}_i\hat{z}_j}\right) = e^{-f^2k_z^2\langle\Delta u_i\Delta u_j\rangle\hat{z}_i\hat{z}_j/2} ,$$

$$\Delta u_i = u_i(\mathbf{x}) - u_i(\mathbf{x}') . \quad (10)$$

To simplify our analysis we also restrict ourselves to the case of locally isotropic turbulent velocity fields¹². Thus the structure tensor $\langle\Delta u_i\Delta u_j\rangle$, which fully describes an isotropic vector field can be expressed via longitudinal D_{LL} and transverse D_{NN} components (Monin & Yaglom 1972)

$$\langle\Delta u_i\Delta u_j\rangle = (D_{LL}(r) - D_{NN}(r))\frac{r_i r_j}{r^2} + D_{NN}(r)\delta_{ik} , \quad (11)$$

where δ_{ik} equals 1 for $i = k$ and zero otherwise. We define z-projection of the velocity structure function as

$$D_z(\mathbf{r}) \equiv \langle\Delta u_i\Delta u_j\rangle\hat{z}_i\hat{z}_j = D_{NN}(r) + [D_{LL}(r) - D_{NN}(r)]\cos^2\theta , \quad \cos\theta \equiv \hat{\mathbf{r}} \cdot \hat{\mathbf{z}} \quad (12)$$

Substituting eqs. (11) and (10) into eq.(7) we obtain:

$$P_s(\mathbf{k}) = \int d^3\mathbf{r} e^{i\mathbf{k}\cdot\mathbf{r}}\xi(r) \exp\left[-\frac{f^2k_z^2D_z(\mathbf{r})}{2}\right] . \quad (13)$$

It is easy to see that the power spectrum above is anisotropic, with velocity mapping having most effect on the modes parallel to the line of sight ($k_z = k$) and not affecting the perpendicular ones ($k_z = 0$).

2.4. Velocity field

If the velocity field is solenoidal¹³ then according to Monin & Yaglom (1972) D_{LL} and D_{NN} are related via a simple relation:

$$D_{NN}(r) = D_{LL}(r) + \frac{r}{2} \frac{d}{dr} D_{LL}(r) . \quad (14)$$

Observational data that we discuss in section 5 corresponds to a power law. This is suggestive that the underlying statistics is also a power-law. For the power-law statistics velocity eq. (14) provides $D_{LL} = 2/(m+2)D_{NN} = Cr^m$.

For potential fields Monin & Yaglom (1972) show that

$$D_{LL}(r) = D_{NN}(r) + \frac{r}{2} \frac{d}{dr} D_{NN}(r) , \quad (15)$$

thus for power-law structure functions $D_{LL} = (1+m/2)D_{NN}$ and again $D_{LL} \sim r^m$.

In general, the velocity field will have both potential and solenoidal components and this introduces an uncertainty of the order unity in the coefficients relating D_{LL} and D_{NN} . This does not change much in our results, and therefore, for the sake of simplicity, doing calculations we shall assume that the velocity field is solenoidal, which probably is not too far from the truth.

The convergence of integrals restricts m to the range $0 < m < 2$. The value $m = 2/3$ is distinct as it corresponds to the Kolmogorov turbulence, but in Appendix B we consider also cases $m = 1/2, 1$. The power spectrum in velocity space is then

$$P_s(\mathbf{k}) = \int d^3\mathbf{r} e^{i\mathbf{k}\cdot\mathbf{r}}\xi(r) \exp\left[-\frac{(k_z\lambda)^2\tilde{D}_z(\mathbf{r}/\lambda)}{2}\right] , \quad (16)$$

$$\tilde{D}_z(\mathbf{r}/\lambda) = (r/\lambda)^m \left(1 + m/2(1 - \cos^2\theta)\right) , \quad (17)$$

¹²The issue of density anisotropy is analyzed in section 6.2 and the data reduction technique dealing with anisotropies is discussed in L95.

¹³Solenoidality of the velocity field follows for the incompressible fluid from the continuity equation.

where the turbulence scale in *velocity* space is

$$\lambda = [f^2 C]^{\frac{1}{2-m}} . \quad (18)$$

This scale depends on the Galactic rotation curve, direction of observations and turbulence intensity. The scale λ corresponds to the scale over which random velocities map density fluctuations. Physically this is the scale at which the velocity dispersion $\sim C\lambda^m$ becomes equal to the squared difference of the regular velocities determined by Galactic rotation (i.e. $f^{-2}\lambda^2$).

While we discuss the properties of the 3D spectrum in velocity space in Appendix B, the 2D spectrum of HI intensity fluctuations available via observations is discussed in the next section.

3. THICK AND THIN SLICING OF DATA CUBES

It is easy to see that a radiointerferometer gets the 2D spectrum of 21 cm intensity (see L95). Therefore it is very important to relate this 2D spectrum to the underlying 3D statistics of turbulence. The velocity resolution of an individual radiointerferometer channel represents the thinnest slicing of the data available. In practice, several channels can be combined to provide a thicker slice (see Green 1993).

Henceforth we use capital letters \mathbf{R} and \mathbf{K} to denote 2D quantities and reserve small letters \mathbf{r} and \mathbf{k} for 3D quantities. In particular, \mathbf{R} is the vector in two dimensional plane orthogonal to the line of sight, and the distance in xyv space is $\mathbf{r}_s^2 = \mathbf{R}^2 + z_s^2$, where z_s is the z-coordinate in velocity space.

An important property of 21 cm emission is that it does not depend on gas temperature (see Spitzer 1978). For negligible self-absorption (see discussion in section 2.1) the HI intensity at the point \mathbf{R} , observed in velocity slice δV , is proportional to the integral of the density over the slice thickness

$$I(\mathbf{R}) \sim \int dz'_s \rho(\mathbf{R}, z'_s) W_e \left[\frac{z_s - z'_s}{\mathcal{L}_{\text{sl}}} \right] . \quad (19)$$

The width of the normalized ($\int dx_s W_e = 1$) experimental window function W_e , \mathcal{L}_{sl} , represents the velocity slice thickness; z_s is the value of the slice central velocity. We expressed both quantities in length units, i.e. $\mathcal{L}_{\text{sl}} \approx f\delta V$, keeping in mind the coordinate transformation (2). The shape of the window function depends on the sensitivity profile and the width of the individual interferometer channel and on how the channels are combined. In idealized case of uniform sensitivity one can consider step-like window $W_e(\Delta z/\mathcal{L}_{\text{sl}}) = 1/\mathcal{L}_{\text{sl}}$ if $|\Delta z| \leq \mathcal{L}_{\text{sl}}/2$ and $W_e = 0$ otherwise. Intensity $I(\mathbf{R})$ implicitly carries dependence on z_s , which we omit for brevity.

The normalized correlation function of intensity fluctuations is

$$\begin{aligned} \langle \delta I(\mathbf{R}_1) \delta I(\mathbf{R}_2) \rangle &\sim \int \int dz'_{s2} dz'_{s1} \langle \delta \rho(\mathbf{R}_1, z'_{s1}) \delta \rho(\mathbf{R}_2, z'_{s2}) \rangle W_e \left[\frac{z_{s1} - z'_{s1}}{\mathcal{L}_{\text{sl}}} \right] W_e \left[\frac{z_{s2} - z'_{s2}}{\mathcal{L}_{\text{sl}}} \right] \\ &= \int \int dz'_{s2} dz'_{s1} \xi_s(\mathbf{R}_1 - \mathbf{R}_2, z'_{s1} - z'_{s2}) W_e \left[\frac{z_{s1} - z'_{s1}}{\mathcal{L}_{\text{sl}}} \right] W_e \left[\frac{z_{s2} - z'_{s2}}{\mathcal{L}_{\text{sl}}} \right] \end{aligned} \quad (20)$$

where δI and $\delta \rho$ mean, respectively, variations of intensity and density. The density correlation function in the velocity space ξ_s is the Fourier transform of the turbulence spectrum $P_s(\mathbf{K}, k_z)$ (see eq. (13)) smoothed by the thermal factor

$$\xi_s(\mathbf{r}_s) = (2\pi)^{-3} \int d^3 \mathbf{k} e^{-i\mathbf{k}\cdot\mathbf{r}_s} P_s(\mathbf{k}) e^{-f^2 k_z^2 v_T^2} \quad (21)$$

The properties of the correlation function are discussed in Appendix C.

The sum of the squared imaginary and real parts of the interferometer visibility function is proportional to the two dimensional spectrum of intensity fluctuations (see L95), which is

$$P_2(\mathbf{K}) \equiv \int d^2 \mathbf{R} e^{i\mathbf{K}\cdot\mathbf{R}} \langle \delta I(\mathbf{R}_1) \delta I(\mathbf{R}_1 + \mathbf{R}) \rangle . \quad (22)$$

Substituting eqs. (20) and (21) into eq. (22) after simple calculations similar to those in Appendix E we derive the expression for $P_2(\mathbf{K})$

$$P_2(\mathbf{K})|_{\mathcal{L}} \sim \frac{1}{2\pi} \int_{-\infty}^{\infty} dk_z P_s(\mathbf{K}, k_z) \tilde{W}_e^2(k_z \mathcal{L}_{\text{sl}}) e^{-f^2 k_z^2 v_T^2} \quad , \quad (23)$$

where $|_{\mathcal{L}}$ reflects the dependence on the slice thickness. $\tilde{W}_e(k_z \mathcal{L}_{\text{sl}})$ is the Fourier transform of the experimental window function. For instance $\tilde{W}_e^2(k_z \mathcal{L}_{\text{sl}}) = 2[1 - \cos(k_z \mathcal{L}_{\text{sl}})] / (k_z \mathcal{L}_{\text{sl}})^2$ for the step-like window.

The effective filter $W(k_z \mathcal{L}_{\text{sl}}, k_z v_T)$ acting on 3D turbulence spectrum in eq. (23) is the product of experimental window function and the thermal term

$$W(k_z \mathcal{L}_{\text{sl}}, k_z v_T) = \tilde{W}_e^2(k_z \mathcal{L}_{\text{sl}}) e^{-f^2 k_z^2 v_T^2} \quad . \quad (24)$$

This demonstrates that thermal dispersion can be treated as part of the experimental velocity window. The effect of velocity slicing δv is similar to the effect of v_T in the sense that they both limit the k_z resolution. Increase of v_T smears the fluctuations. Thus we may expect the fluctuations from colder, $v_T < \delta v$, parts of the medium to dominate over the contribution from warmer, $v_T > \delta v$, parts. The exact criterion when this is true is given below.

At small k_z we have $W \propto 1 - k_z^2 (\tilde{W}_e^{2''}(0) \mathcal{L}_{\text{sl}}^2 + 2f^2 v_T^2) / 2$, thus the characteristic scale of the window can be defined by an effective slice thickness

$$\mathcal{L} = 2(\tilde{W}_e^{2''}(0) \mathcal{L}_{\text{sl}}^2 + 2f^2 v_T^2)^{1/2} = 2f(\tilde{W}_e^{2''}(0) \delta v^2 + 2v_T^2)^{1/2} \quad . \quad (25)$$

This is the customary definition of a characteristic scale as twice the value of k_z^{-1} at which the filter value drops by a factor of two of its maximum. This approximately corresponds to the full width at half maximum of the window in velocity space and is the effective width of the velocity slice. In what follows we denote the window function given by eq. (24) by $W(k_z \mathcal{L})$ and disregard its dependence on v_T when it is possible. In section 4.3, we, however, will have to treat the dependence of \mathcal{L} on v_T in order to determine the relative contribution of the warm and cold HI.

For step-like experimental window, $\tilde{W}_e^{2''}(0) = 1/6$. In this case thermal velocity dispersion has much more profound effect than the averaging over the velocity channel of similar thickness. This is due to relatively weak cutoff in Fourier space provided by step-like averaging in velocity slice.

As long as the exact shape of the high k_z cutoff by the window function is not important, using effective slice thickness fully accounts for the effect of finite gas temperature. From now on we shall mean ‘effective’ everywhere we speak about slice thickness.

The thinner is the velocity slice \mathcal{L} , the closer to unity is the window W over larger range of k_z and more 3D modes contribute to 2D spectrum.

We shall call a slice *thin*, when the $W(k_z \mathcal{L})$ can be approximated by unity over all k_z of interest and the one of *thick*, when it is important that at high k_z the function $W(k_z \mathcal{L})$ decreases. Therefore when the slice is *thin* eq. (23) gives¹⁴

$$P_2(\mathbf{K})|_t \approx \frac{1}{2\pi} \int dk_z P_s(\mathbf{K}, k_z) \quad , \quad (26)$$

where $|_t$ denotes that the slice is thin while in the limit of a *thick* slice the exact expression for the window function $W(k \mathcal{L})$ (i.e. eq. (24)) should be used. Obviously enough, whether the slice is thin or thick depends not only on \mathcal{L} but also on the properties of $P_s(\mathbf{K}, k_z)$. The exact criteria for slices to be thin and thick are discussed in the next section.

¹⁴The intuitive notion of the thin slice is hardly associated with the integral over spectrum. Note, however, that the integral is taken in k -space and, for instance, a thin sheet in a real space corresponds to an integral in k -space. A different way of understanding eq. (26) is to consider randomly moving 3D waves that produce a pattern corresponding to the wavevector \mathbf{K} on their intersection of the plane. Obviously enough, various 3D waves with $\mathbf{k} = (\mathbf{K}, k_z)$ contribute to the pattern. Integration over k_z in eq. (26) reflects this.

One expects different behavior of resulting 2D spectrum P_2 depending on a slice being *thin* or *thick*. To clarify this distinction, let us consider the density power-law 3D spectrum $P_s(\mathbf{K}, k_z) \propto (|\mathbf{K}|^2 + k_z^2)^{n/2}$, $n < -1$ that is *not* subject to a velocity mapping. For this simple case $P_s(\mathbf{K}, k_z)$ is nearly constant if $k_z < |\mathbf{K}|$ and $\propto k_z^n$ if $k_z > |\mathbf{K}|$. This fall-off at high k_z (n is negative) amounts to a cut-off of the integral $\int_0^\infty dk_z P_s(\mathbf{K}, k_z) \approx \int_0^{|\mathbf{K}|} dk_z P_s(\mathbf{K}, k_z)$ at $k_z \approx |\mathbf{K}|$ (assuming, as we did, $n < -1$). Correspondingly, if $\mathcal{L}|\mathbf{K}| \ll 1$ the window function is unimportant and the slice is *thin*, while the slice is *thick* when $\mathcal{L}|\mathbf{K}| \gg 1$. In other words, the transition between *thick* and *thin* slices occurs when we consider wavelengths longer or shorter than slice thickness. For the thick slice, the contribution to the integral (23) for the case considered mostly comes from the $k_z \sim 0$ modes i.e.

$$P_2(\mathbf{K})|_{\mathcal{T}} \approx P_s(\mathbf{K}, \bar{k}_z) \int dk_z W(k_z \mathcal{L}) / 2\pi \approx \mathcal{L}^{-1} P_s(\mathbf{K}, 0) \quad , 0 \leq \bar{k}_z < 1/\mathcal{L}, \quad (27)$$

where $|_{\mathcal{T}}$ denotes that the slice is thick, and this result corresponds to the finding in L95. The result can be easily understood. For sufficiently steep spectra ($n < -1$) integration over z corresponds to choosing $k_z = 0$ mode in the Fourier space. Thus the 2D intensity spectrum and the underlying 3D density spectrum with $k_z = 0$ should be identical.

Thus, the asymptotics of the 2D power spectrum produced by integrating density fluctuations along a line of sight are

$$P_2(\mathbf{K}) \propto \begin{cases} |\mathbf{K}|^n, & \mathcal{L}|\mathbf{K}| \gg 1 \\ |\mathbf{K}|^{n+1}, & \mathcal{L}|\mathbf{K}| \ll 1 \end{cases} \quad (28)$$

However, the rule of transition between *thin* and *thick* slices gets modified when we consider the emissivity power spectrum in velocity space. In the presence of velocity mapping (see eq. (2)) an additional scale¹⁵ λ (see eq. (7)) appears. This alters the wavenumber $|\mathbf{K}|$ at which the transition between the *thin* and *thick* slices occurs.

The *thin*-slice expression for 2D spectrum in the velocity space follows from eq. (26) with 3D kernel given by eq. (16)

$$P_2(\mathbf{K})|_t \approx \frac{1}{(2\pi)^{1/2} \lambda} \int d^3 \mathbf{r} e^{i\mathbf{K} \cdot \mathbf{R}} \frac{\xi(r)}{\tilde{D}_z(\mathbf{r}/\lambda)^{1/2}} \exp \left[-\frac{z^2}{2\lambda^2 \tilde{D}_z(\mathbf{r}/\lambda)} \right] \quad (29)$$

The exact relation between $P_2(\mathbf{K})$ and the underlying velocity and density statistics depends on whether the density spectrum of HI is shallow or steep. In the next section we discuss these two cases separately.

4. TWO DIMENSIONAL SPECTRA

Below we consider the distribution of density dominated (a) by fluctuations at small scales and (b) by fluctuations at large scales. As we mentioned earlier, we limit our discussion to the power-law spectra both because observations suggest power-law dependences (see Green 1993, Stanimirovic et al 1999). If future research suggests a different dependences for interstellar statistics, our formulae can be used to fit the data. We show that in terms of power-law spectra case (a) corresponds to a power-law index $n > -3$ and case (b) to $n < -3$.

4.1. Short-wave dominated spectrum of density field

To describe the statistical properties of the density fluctuations dominated by short wavelengths, we use power-law correlation functions of *over-density*:

$$\xi(r) = \langle \rho \rangle^2 \left(1 + \left(\frac{r_0}{r} \right)^\gamma \right), \quad \gamma > 0 \quad . \quad (30)$$

¹⁵If the underlying 3D spectrum has several built-in scales, detailed analysis can distinguish between several intermediate asymptotics.

The power-law part of the correlation corresponds to the 3D power-law spectrum

$$P(k) \propto k^n, \quad n = \gamma - 3 > -3 \quad . \quad (31)$$

The unity term in eq. (30) reflects the fact that *density* has non-zero mean value. After Fourier transformation this term leads to a delta function term at $\mathbf{k} = 0$ added to the power spectrum. The correlation scale r_0 gives us the second parameter of the problem (the first one being λ).

Two terms in the expression for correlation function lead to the correspondent split of the power spectrum in velocity space into two parts. We show in the Appendix B that the 3D power spectrum in velocity space can be presented as

$$P_s(|\mathbf{K}|, k_z) = \langle \rho \rangle^2 [P_v(|\mathbf{K}|, k_z) + P_\rho(|\mathbf{K}|, k_z)] \quad , \quad (32)$$

where we introduced a notation

$$P_v(|\mathbf{K}|, k_z) = \int d^3 \mathbf{r} e^{i\mathbf{k} \cdot \mathbf{r}} \exp \left[-\frac{(k_z \lambda)^2 \tilde{D}_z(\mathbf{r}/\lambda)}{2} \right] \quad , \quad (33)$$

$$P_\rho(|\mathbf{K}|, k_z) = \int d^3 \mathbf{r} e^{i\mathbf{k} \cdot \mathbf{r}} (r_0/r)^\gamma \exp \left[-\frac{(k_z \lambda)^2 \tilde{D}_z(\mathbf{r}/\lambda)}{2} \right] \quad . \quad (34)$$

In eq. (32) $P_v(\mathbf{k})$ is the emissivity spectrum in velocity space arising from random velocity fluctuations in an incompressible fluid and in terms of mathematics arises from the unity term (mean density) in eq. (30), while $P_\rho(\mathbf{k})$ describes the spectrum of emissivity fluctuations arising from both velocity and density fluctuations. Formally $P_\rho(\mathbf{k})$ arises from velocity mapping acting upon the density fluctuations given by $(r/r_0)^\gamma$ term in eq. (30). As expected, the P_v term has a δ -function behavior at $k = 0$, but in velocity space it is also non-vanishing for $k > 0$. As we mentioned earlier even uniformly distributed in space, but turbulently moving incompressible fluid produce fluctuating emission (given by $P_v(\mathbf{k})$) when observed in velocity slice of finite thickness.

We derive the asymptotics for P_v and P_ρ in Appendix B. The main result is that the velocity mapping leads to the rapid cutoff of modes with large k_z component of the wave vector. Both P_ρ and P_v falls sharply ($\propto k_z^{-2\alpha/m}$, where α is 3 for P_v or $-n$ for P_ρ) for $k_z \gg \lambda^{-1}(k\lambda)^{m/2}$, $k^2 = \mathbf{K}^2 + k_z^2$. This implicitly defines the cutoff scale k_z^c which can be approximated as $k_z^c = \lambda^{-1}(1 + |\mathbf{K}|\lambda)^{m/2}$.

We will see that P_v and P_ρ emerge, although in another combination, when the density spectrum is long-wave dominated. Thus, below, we formulate a *general criterion* for the slice to be *thin* or *thick* in the presence of velocity mapping.

As we discuss in section 5, for scales of observational interests $|\mathbf{K}|\lambda \gg 1$. For these modes $k_z^c \approx \lambda^{-1}(|\mathbf{K}|\lambda)^{m/2} < |\mathbf{K}|$, since $m < 2$. This strongly affects the integration in eq. (23). Indeed, one can assume that the window function $W(\mathcal{L}k_z) \approx 1$ as long as $\mathcal{L}k_z^c < 1$. In particular, the slice remains *thin* for much larger $|\mathbf{K}|$ than one would expect from the example of power-law spectrum unmodified by the velocity mapping (see eq. (28)). Now, given $|\mathbf{K}|\lambda \gg 1$, the transition between the *thin* to *thick* slice regimes is

$$\begin{aligned} \textit{thin slice} : & \quad \mathcal{L}/\lambda \cdot (|\mathbf{K}|\lambda)^{m/2} \ll 1 \\ \textit{thick slice} : & \quad \mathcal{L}/\lambda \cdot (|\mathbf{K}|\lambda)^{m/2} \gg 1 \end{aligned} \quad (35)$$

The *thin*-slice asymptotics is achieved when the first condition is satisfied due to very steep cutoff of 3D spectrum at high k_z . In other words, due to a rapid decrease of 3D spectrum P_s the window function can be ignored over the whole range of k_z . The last inequality essentially gives us the *necessary* condition for the variations of the window function to be important. To appreciate the effect of the velocity mapping let us rewrite it as $\mathcal{L}|\mathbf{K}| > (|\mathbf{K}|\lambda)^{1-m/2} \gg 1$. This is to be compared with *thick slice* condition $\mathcal{L}|\mathbf{K}| > 1$ which would take effect if there is no velocity term, $\lambda \rightarrow 0$ (combined rule $\mathcal{L}|\mathbf{K}| > \max(1, (|\mathbf{K}|\lambda)^{1-m/2})$ is valid for any λ). For the wavenumber $|\mathbf{K}| = (10 \text{ pc})^{-1}$, typical velocity turbulence scale $\lambda = 3.5 \text{ kpc}$

(see Section 5) and $m = 2/3$ we thus need $\mathcal{L} > 500$ pc for slice to be *thick*, which is fifty times larger than Eq. (28) suggests. Indeed, according to Eq. (28) $\mathcal{L} > |\mathbf{K}|^{-1} = 10$ pc is sufficient for the slice to be thick if the velocity field is absent.

The separation between *thin* and *thick* regimes is intuitively clear if rewritten in physical units. Substituting λ from eq. (18) and expressing slice thickness through the width of window function, which for $v_T = 0$ is proportional to the width of the interferometer channel δV , $\mathcal{L} = f\delta V$ we obtain

$$\begin{aligned} \textit{thin slice} : & \quad C|\mathbf{K}|^{-m} \gg \delta V^2 \\ \textit{thick slice} : & \quad C|\mathbf{K}|^{-m} \ll \delta V^2 \end{aligned} \quad (36)$$

In other words, if the velocity dispersion Cr^m on the scale $|\mathbf{K}|^{-1}$ is larger than the squared width of the channel¹⁶ (in velocity units) the slice is *thin*. If the opposite is true – the slice is *thick*. We stress, that the critical wavelength depends only on the width of the interferometer channel and the amplitude of velocity turbulence, but not on the direction of observations or the actual physical thickness of the slice involved (al long as $|\mathbf{K}|\lambda \gg 1$). To observe the transitions between the two regimes one can either vary δV or $|\mathbf{K}|$. We show in Appendix E that the criterion (36) is quite general and applicable not only to the Galaxy but to individual clouds and external galaxies.

The 2D spectrum of intensity fluctuations in a velocity slice of data can be obtained using eq. (23). It follows from eq. (32) that

$$P_2(|\mathbf{K}|) = \langle \rho \rangle^2 [P_{2v}(|\mathbf{K}|) + P_{2\rho}(|\mathbf{K}|)] \quad , \quad (37)$$

where

$$P_{2v}(\mathbf{K})|_{\mathcal{L}} \sim \frac{1}{2\pi} \int_{-\infty}^{\infty} dk_z P_v(\mathbf{K}, k_z) W(k_z \mathcal{L}) \quad , \quad (38)$$

and

$$P_{2\rho}(\mathbf{K})|_{\mathcal{L}} \sim \frac{1}{2\pi} \int_{-\infty}^{\infty} dk_z P_\rho(\mathbf{K}, k_z) W(k_z \mathcal{L}) \quad , \quad (39)$$

The calculation of appropriate integrals is straightforward using the asymptotics for 3D spectra P_v and P_ρ obtained in Appendix B. In Table 1 we present asymptotical formulae for $P_{2\rho}$ and P_{2v} spectra in a *thin* and a *thick* slice regimes under the assumption $|\mathbf{K}|\lambda \gg 1$. $P_{2\rho}$ and P_{2v} also appear in the case of long-wave dominated density fluctuations and therefore our results are quite general.

In the regime of a *thick* slice Table 1 shows that the power-law indexes of the 2D spectrum and the underlying 3D density spectrum coincide. This is the regime considered in L95. If the slice is *thin*, the 2D spectrum index becomes shallower, i.e. $n + m/2$. However this spectrum is still steeper than the spectrum of density in a *thin* slice in the absence of velocity modulations. Indeed, in the latter case eq. (28) predicts the index $n + 1 > n + m/2$ for $m < 2$. This *thin*- slice behavior can be immediately found from the integral representation given by eq. (29). As can be easily shown, at high $|\mathbf{K}|$ the exponential factor can be set to unity, so

$$P_2(\mathbf{K})|_t \approx \frac{1}{(2\pi)^{1/2}\lambda} \int d^3\mathbf{r} e^{i\mathbf{K}\cdot\mathbf{R}} \frac{\xi(r)}{\tilde{D}_z^{1/2}(\mathbf{r}/\lambda)} \quad (40)$$

An extra factor $D_z^{1/2}(\mathbf{r}) \propto C^{1/2}r^{m/2}$ is responsible for the change of slope of the spectrum due to velocity effect.

Note that in a *thin* slice P_{2v} behaves as a density part $P_{2\rho}$ taken with $n = -3$. Comparing expression for $P_{2\rho}$ rewritten as $P_{2\rho} = S_{nm}(|\mathbf{K}|r_0)^{3+n}(|\mathbf{K}|\lambda)^{-3+m/2}$ with the formula for P_{2v} shows that for short-wave dominated spectra $n > -3$ the density part is always dominant over P_{2v} at wavelength shorter

¹⁶Here, for the sake of simplicity, we talk about measurements for which the thickness of the slice is determined by the velocity channel of the telescope. In reality, data from many channels can be added to produce a thicker slice (see section 6). Moreover, in most cases v_T contribution is important in eq. (25) and in more precisely $\delta V = 0.5(\tilde{W}_e^{2''}(0)\delta v^2 + 2v_T^2)^{1/2}$. Generalizations of our criterion to these cases are trivial.

	thick slice	thin slice
	$\mathcal{L}/\lambda \cdot (\mathbf{K} \lambda)^{m/2} \gg 1$	$\mathcal{L}/\lambda \cdot (\mathbf{K} \lambda)^{m/2} \ll 1$
$\lambda^{-2}P_{2\rho}(\mathbf{K}) :$	$A_n \cdot (\lambda/\mathcal{L}) \cdot (r_0/\lambda)^{3+n} \cdot (\mathbf{K} \lambda)^n;$	$S_{nm}(r_0/\lambda)^{3+n} \cdot (\mathbf{K} \lambda)^{n+m/2}$
$\lambda^{-2}P_{2v}(\mathbf{K}) :$	$B_m \cdot (\lambda/\mathcal{L})^3 \cdot (\mathbf{K} \lambda)^{-3-m};$	$S_{-3m} \cdot (\mathbf{K} \lambda)^{-3+m/2}$

TABLE 1

ASYMPTOTICS OF THE 2D SPECTRUM IN THE *thin* AND *thick* VELOCITY SLICES FOR $|\mathbf{K}|\lambda \gg 1$. NUMERICAL CONSTANTS A_n , B_m AND S_{nm} ARE GIVEN IN APPENDIX A. IN APPENDIX E WE SHOW THAT THESE RESULTS ARE APPLICABLE TO INDIVIDUAL CLOUDS PROVIDED THAT THE CLOUD SIZE IS USED INSTEAD OF λ .

than the density correlation length $|\mathbf{K}|r_0 > 1$. The density term $P_{2\rho}$ is also dominant for *thick* slices. Indeed,

$$\frac{P_{2\rho}}{P_{2v}} \approx (|\mathbf{K}|r_0)^{3+n} \left[\left(\frac{\mathcal{L}}{\lambda} \right)^2 (|\mathbf{K}|\lambda)^m \right] \gg 1, \quad (41)$$

as shallow density with $n > -3$ and the terms in the second bracket $\gg 1$ for a thick slice. In this regime the velocity part has an extra $(\lambda/\mathcal{L})^2$ factor and extra damping $(|\mathbf{K}|\lambda)^{-m}$.

The magnitude of $P_{2v}(\mathbf{K}, k_z)$ is more tangible than one might suggest in an analogy with eq. (27). The reason is that $P_{2v}(\mathbf{K}, k_z)$ is a growing function of k_z up to $k'_z = \lambda^{-1} \max[1, (|\mathbf{K}|\lambda)^{m/2}]$ (see Table 2 in Appendix B). This is the case where the exact shape of the fall-off of the window $W(\mathcal{L}k_z)$ is important. Typically if $W(\mathcal{L}k_z)$ falls fast at $k_z > \mathcal{L}^{-1}$ we have

$$\lambda^{-2}P_{2v}(|\mathbf{K}|) \propto \lambda \int_0^{1/\mathcal{L}} dk_z \frac{(k_z \lambda)^2}{(k \lambda)^{3+m}} \propto (\lambda/\mathcal{L})^3 (|\mathbf{K}|\lambda)^{-3-m} \quad (42)$$

Peculiar is the case of step-like uniform window, which falls off only as $1/(k_z \mathcal{L})^2$, then

$$\lambda^{-2}P_{2v}(|\mathbf{K}|) \propto \int_0^{(|\mathbf{K}|\lambda)^{m/2}} d(\lambda k_z) \frac{(k_z \lambda)^2}{(k \lambda)^{3+m}} \frac{1}{(k_z \mathcal{L})^2} \propto (\lambda/\mathcal{L})^2 (|\mathbf{K}|\lambda)^{-3-m/2} \quad (43)$$

Our numerical results have been obtained for this case.

Details of the transition from *thin* to *thick* slicing as \mathcal{L} increases require numerical study. The results, plotted in Figure 1, confirm the accuracy of our analytical estimates. Our calculations show how with the increase of slice thickness the spectral index of $P_{2\rho}$ steepens from the value $n + m/2$, characteristic to thin slice, towards the value n measured in thick slices. The transition scale between these two regimes is significantly increased as the result of velocity fluctuations. For thin slices and large \mathbf{K} the $P_{2\rho}$ spectrum depends on both velocity and density fluctuations. The pure velocity term P_{2v} is always subdominant at short wavelengths.

All in all, on short wavelengths $|\mathbf{K}|\lambda \gg 1$ thick velocity slicing of 21 cm data cubes provides the spectrum $|\mathbf{K}|^n$, while thin slicing provides $|\mathbf{K}|^{n+m/2}$. Therefore if density statistics is dominated by small scale fluctuations, interferometers can provide us both with density and velocity statistics; the density spectral index being obtained from thick slices, and combining this with the thin slice data one can obtain the velocity spectral index m .

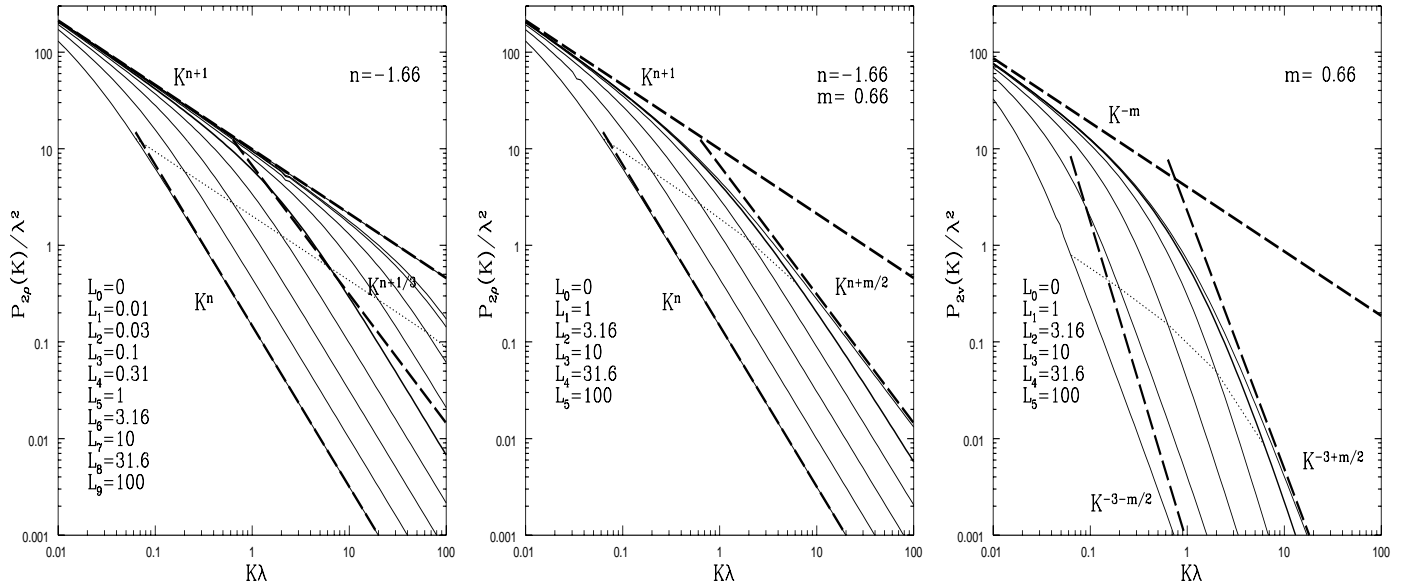


FIG. 1.— Two dimensional power spectrum measured in a slice of variable thickness $L = \mathcal{L}/\lambda$ (upper curves correspond to smaller L_i). Left panel shows $P_2(|\mathbf{K}|)$ in the absence of velocity mapping. The middle and the right panels correspond to density $P_{2\rho}$ and velocity P_{2v} terms. The upper dashed lines show the *thin* slice power-law asymptotics described in Table C3; for comparison the short-wave $P_{2\rho}$ slope is also shown in the left panel. The curve of enhanced weight corresponds to $L = 1$. The *thick* slice asymptotics are accurate below the dotted line.

4.2. Long-wave dominated spectrum of density field

Our analysis above does not cover $\gamma < 0$ and $n < -3$. This is the regime dominated by large-scale density fluctuations that we consider in this section.

Kolmogorov turbulence is often assumed to be valid not only for the velocity but also for the density¹⁷. This type of turbulence corresponds to $\gamma = -2/3 = -m$, $n = -11/3$. For $\gamma < 0$ we formally substitute in Eq. (16)

$$\xi(r) = d(\infty)[1 - d(r)/d(\infty)] \quad , \quad (44)$$

where $d(r)$ is a structure function¹⁸ of density

$$d(r) = \langle (\rho(\mathbf{x} + \mathbf{r}) - \rho(\mathbf{x}))^2 \rangle \quad . \quad (45)$$

Real world structure functions do not grow infinitely and therefore we have to introduce a cutoff at some large scale. If the cut-off happens at r_c then for the long-wave dominated turbulence ($\gamma < 0$)

$$d(r) = d(\infty) \frac{r^{-\gamma}}{r^{-\gamma} + r_c^{-\gamma}} \quad , \quad (46)$$

and the correlation function is

$$\xi(r) = \frac{d(\infty)}{2} \frac{r_c^{-\gamma}}{r^{-\gamma} + r_c^{-\gamma}} \quad . \quad (47)$$

For simplicity¹⁹, further on we assume that the structure functions of velocity and density have the cut-off at the same value of r_c . Below we show that our final results marginally depend on a particular

¹⁷This is exactly true for the density of a passive contaminant transported by the Kolmogorov velocity field. It is not *a priori* clear that such a treatment is applicable to HI.

¹⁸We could start from the structure functions from the very beginning but we preferred to use correlation functions to make our presentation more uniform.

¹⁹This is a consistent assumption for the Kolmogorov density turbulence.

value of r_c as long as r_c is much larger than the turbulence scales under study, i.e. $|\mathbf{K}|r_c \gg 1$. Similarly, it is possible to show that in the presence of two different cut-off scales $r_{1c} < r_{2c}$ the results do not depend on either scale provided that $|\mathbf{K}|r_{1c} \gg 1$.

Observations indicate that the amplitude of random velocity is high enough, so that $\lambda > r_c$ (see section 5). Thus we are predominantly interested in the short-wave regime $|\mathbf{K}|^{-1} < r_c < \lambda$.

For sufficiently small $r \ll r_c$ eq. (47) gives

$$\xi(r) \approx \frac{1}{2}d(\infty)(1 - [r/r_c]^{-\gamma}) \quad (48)$$

Note that in eq. (48) r_c plays the role of r_0 in eq. (30). Both r_c and r_0 are the scales at which most of the energy of the field is stored. It is straightforward to show that at short waves $|\mathbf{K}|r_c > 1$ eq. (48) entails

$$P_2(|\mathbf{K}|) \approx \frac{1}{2}d(\infty) [P_{2v} + P_{2\rho}] \quad , \quad (49)$$

where $P_{2\rho}$ coincides with the definition in section 4.1 if a change $r_c \rightarrow r_0$ is made. P_{2v} arises from the unity term in the definition of correlation functions and therefore is identical to that in section 4.1. Eq. (49) is an analog of eq. (37) for the case of a density field dominated by large-scale fluctuations. The comparison between the two reveals a substantial difference between the two regimes. Note, that by construction $P_{2\rho}$ is the only part which carries the information about the index of underlying density statistics²⁰. The other term, namely, P_{2v} arises purely from velocity. Notice, that in this case the variation of the amplitude $d(\infty)$ of the density fluctuations in xyz space affects P_{2v} and $P_{2\rho}$ (see eq. (49)) in the same way. Asymptotics of P_{2v} and $P_{2\rho}$ are given by Table 1 provided that r_c is used instead of r_0 in the expression for $P_{2\rho}$.

The feasibility of extracting the density statistics from the observable emissivity spectrum depends on the thickness \mathcal{L} of the data slice, which governs the relative magnitude of P_{2v} and $P_{2\rho}$ terms. In a *thin* slice, i.e when $(\mathcal{L}/\lambda) \cdot (|\mathbf{K}|\lambda)^{m/2} > 1$, a comparison between P_{2v} and $P_{2\rho}$ is similar to that carried out in the previous section. It shows that for $n < -3$ P_{2v} always dominates if $|\mathbf{K}|r_c > 1$. In *thick* slice, eq.(42, P_{2v} has the same spectral index as $P_{2\rho}$ but its amplitude differs by $(\lambda/\mathcal{L})^2$. $P_{2\rho}$ dominates when

$$\mathcal{L}/\lambda > (r_0/\lambda)^{m/2} \quad (50)$$

This condition does not qualitatively change when thermal line broadening is taken into account. In general, for $\mathcal{L} \gg \lambda$ the density spectrum should be observable.

It is clear that sufficiently weak velocity turbulence cannot distort the density statistics. Our formulae confirm this intuitive prediction. As the level of velocity turbulence decreases so does the scale λ given by eq. (18). As the result \mathcal{L} for very weak turbulence becomes much greater than λ and therefore the density statistics reveals itself.

Thus we can summarize that when $\mathcal{L} < \lambda$ the velocity term dominates, producing universal spectral slope independent of the underlying density slope n . This means that for the *thick* slices the expected slope is $-3 - m/2$ and for *thin* slices the slope is $-3 + m/2$. If the turbulent velocity as index $m = 2/3$ (the Kolmogorov index), the slope is equal to $-8/3$ if the slice is *thin* and steepens to $-10/3$ for thicker slices.

The effect of velocity mapping on the density power spectrum is illustrated in Figure 2. An additional asymptotics, namely $K^{-4/3}$, arises from the evident expansion of eq. (47) for $r \gg r_c$. In this regime density fluctuations dominate those of intensity.

There may be an element of confusion since ‘‘Kolmogorov’’²¹ density fluctuations in the absence of velocity mapping will also produce $n = -8/3$ spectrum in a thin slice. However, as Figure 2 demonstrates, in the regime when random velocities are large, it is the velocity term that dominates for large $|\mathbf{K}|$. The

²⁰The amplitude of $P_{2\rho}$ for $n < -3$ is negative and this compensates for a minus sign in eq.(49).

²¹We emphasize that the name does not imply the actual connection to the picture of the Kolmogorov energy cascade, but only to the particular power index.

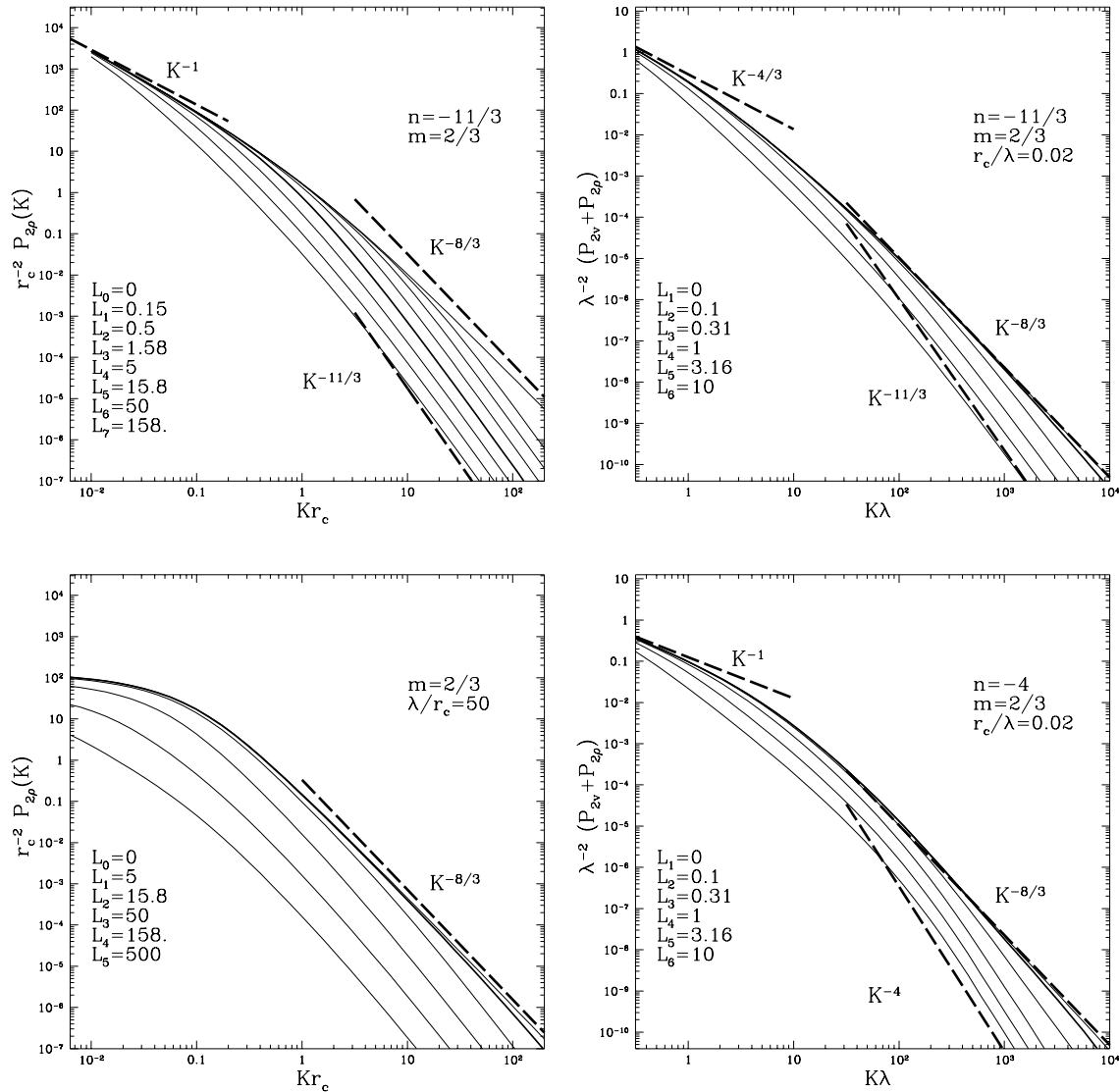


FIG. 2.— Two dimensional power spectrum for “Kolmogorov” turbulence (which does not mean more that the statistics of density and velocity have the Kolmogorov indexes $m = -\gamma = 2/3$) measured in a slice of variable thickness $L = \mathcal{L}/\lambda$ (upper curves correspond to smaller L_i). The ratio $\lambda/r_c = 50$ is fixed. Upper left panel shows $P_2(|\mathbf{K}|)$ when the velocity mapping is absent. All quantities are expressed in units of r_c for this panel. The bottom left panel presents the density P_{2v} term arising from velocity fluctuations only. The upper right panel shows $P_{2v} + P_{2p}$ when both velocity and density are “Kolmogorov”. The dashed lines show power-law asymptotics described in detail in Section 4. Heavy line corresponds to the slice thickness $\mathcal{L} = 0.1\lambda$. The bottom right panel repeats the previous calculations but for $n = -4$. This confirms that in the relatively *thin* slice $\mathcal{L} < \lambda$ both $n = -11/3$ and $n = -4$ cases, irrespectively of n have slope and amplitude determined by velocity fluctuations, as comparison with bottom left panel reveals. The slope is equal to $-8/3$, if the slice is *thin* i.e. $(\mathcal{L}/\lambda)|(\mathbf{K}|\lambda)^{m/2} < 1$, and tends to $-10/3$ for thicker slices. Only slices much thicker than the velocity scale, i.e. $\mathcal{L} \gg \lambda$, reveal the underlying density spectrum.

fact that changes of underlying density spectrum do not alter the observed spectrum for $|\mathbf{K}r_c| \gg 1$ and $\mathcal{L}/r_c < 1$ confirms our claim (see Figure 2).

Now it is time to address the question whether our results depend on the cut-off size r_c . For this purpose we plot the results of calculations for very different values of r_c/λ in Figure 3. It is easy to see that only marginal dependence of the spectral slope on r_c exists for sufficiently large values of $|\mathbf{K}|$.

All in all, in the case of long-wave dominated density statistics both thin and thick slices provide velocity spectral index. To determine the density spectral index one should use *very thick* slices with $\mathcal{L} > \lambda$. Only then the emissivity spectrum begins to reflect the index of the actual HI spectrum

of density (i.e. the density spectrum in Galactic coordinates). The regimes of long and short-wave dominated spectra may be distinguished by varying the thickness of velocity slices.

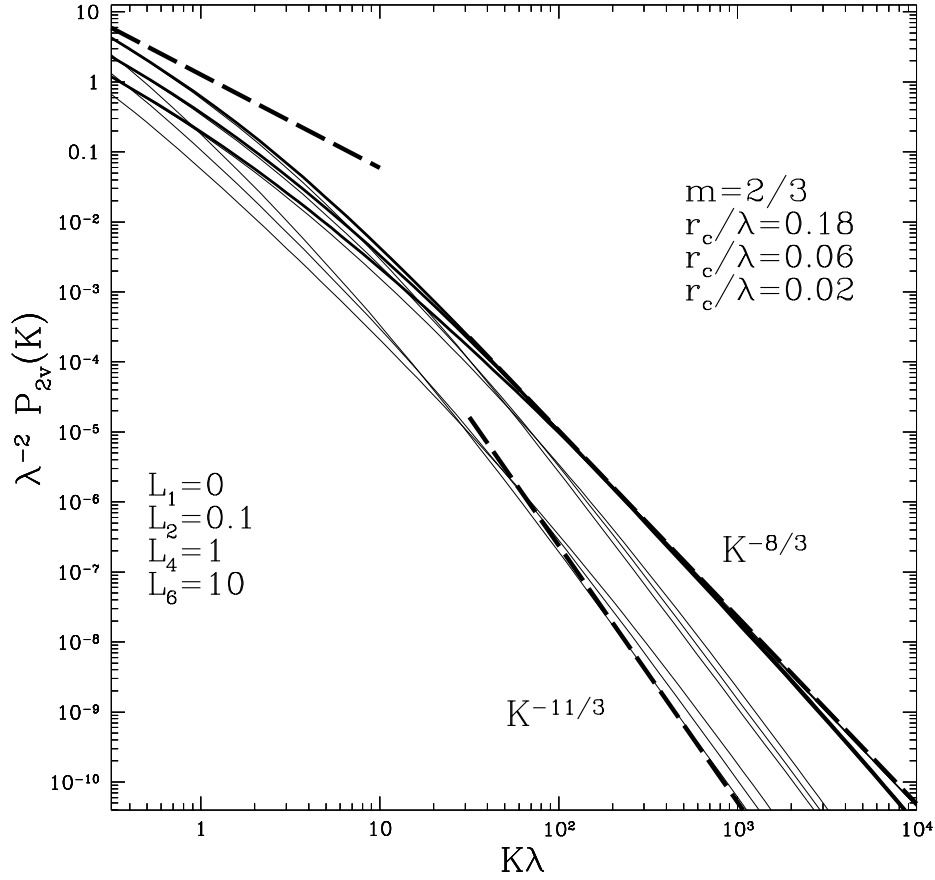


FIG. 3.— Dependence of the two dimensional power spectrum on the structure function cutoff r_c . The results for four values of the slice thickness $L = \mathcal{L}/\lambda$ and three values of r_c are shown. In shortwave regime $|\mathbf{K}|r_c > 1$ 2D spectrum is completely insensitive to r_c for *thin* slice and exhibit only minor dependence on r_c if slice is *thick*. The latter dependence reflects the fact that *thick* asymptotics is achieved a bit later for smaller value of r_c .

4.3. Warm and Cold HI

When we deal with cold ($T \approx 100K$) HI, the turbulent velocity is supersonic, while for warm ($T \approx 6000 K$) HI the turbulent velocity is comparable with the thermal velocity. Our studies above dealt with supersonic turbulence and the effect of the thermal velocities was shown to be equivalent to increasing the thickness of the slice from $\sim \delta V$ to $\sim 2 * (\delta v^2/6 + 2v_T^2)^{1/2}$ (see section 3, we use $W_e'' = 1/6$ assuming step-like experimental window). As a consequence there is no point of getting experimental velocity slices narrower than $\sqrt{12}v_{T,cold} \approx 2.6km/s$. For warm HI the turbulence corresponds to the Mach number of the order of unity and the minimal thickness of the slice is $\gtrsim 17 km/s$. What are the observational consequences of this?

First of all, we may attempt to estimate the actual temperature of HI. We calculated how spectra should change with the thickness of the velocity slice. When $\delta v \gg v_T$ the change of the δv should entail the corresponding change in the effective slice thickness. However, as δv approaches v_T a further increase of the instrument velocity resolution (i.e. decreasing δv) will not result in the change of the power slope. In the medium with a few HI phases having different temperatures T_i the transitions will happen for a number of $\delta_i V = 3.5v_{T,i}$. Modulations of power-law spectral index as a function of δV

should reflect the distribution of temperatures of HI components along the line of sight. We shall discuss the particular technique of probing HI temperature distribution elsewhere.

For the generally accepted picture of the mixture of warm and cold components the power spectrum can be presented as the sum of a three:

$$P_2(\mathbf{K}) = P_{2(cold)}(\mathbf{K}) + P_{2(warm)}(\mathbf{K}) + P_{2(warm-cold)}(\mathbf{K}) \quad (51)$$

where the part $P_{2(warm-cold)}(\mathbf{K})$ arises from correlations between warm and cold components. Note that the minimal effective thickness of the slice for the warm component is ≈ 20 km/s. When δv approaches this thickness we expect to see variations of the spectral index if the warm gas constitutes a substantial fraction of the total HI. As mentioned above, this potentially may be used to determine the relative abundance of the components.

Assume, for the sake of simplicity, that the mass fraction of the cold and warm media are comparable and the same is true for the amplitudes of the three dimensional spectra $P_{s(warm)}$ and $P_{s(cold)}$. When the experimental slice width δV is smaller than $\sqrt{12}v_{T(warm)}$ the the ratio of cold to warm contributions $P_{s(warm)}/P_{s(cold)}$ as a function of wavenumber \mathbf{K} will be constant of order unity at long wavelength $\mathbf{K} \ll (C^2/3.5v_{T(warm)})^{1/m}$ (see criterion (36)), then fall off as $K^{-2/m}$ until $\mathbf{K} \approx (C^2/\delta V)^{1/m}$ and be constant again but suppressed as $\sim \delta V/3.5v_{T(warm)}$ at shorter wavelength (if $\delta V < 3.5v_{T(cold)}$), until the maximum suppression $\sim v_{T(cold)}/v_{T(warm)}$ is reached)²². These three regimes correspond to wavelengths for which effective slice is, first, *thin* for both cold and warm component, then still *thin* for cold, but already *thick* for the warm one and, finally, *thick* for both contributions. Addressing the actual Galactic HI data in Fig. 4 we may see that the slicing is frequently thin for cold HI and thick for warm HI. As δV increases above thermal velocity of warm component, shortwave relative suppression of contribution from warm HI disappears.

In reality $P_{s(warm)}$ and $P_{s(cold)}$ may have different amplitudes and even different spectral slopes. Moreover, the mass fraction in those component may vary. The variations P_2 with the slice thickness may allow to determine the characteristics of the turbulence in the multiphase media.

The $P_{2(warm-cold)}$ contribution arises from the correlations between fluctuations in warm and cold media. The density fluctuations are spatially separated in two media and therefore their correlation is likely to be negligible. We may not be so sure about the velocity fluctuations as cold and warm gas may participate in a coherent motions. It may be shown, however, that the difference between $v_{T(warm)}$ and $v_{T(cold)}$ will suppress a possible contribution from $P_{2(warm-cold)}$ in a manner similar to the suppression of $P_{2(warm)}$.

5. OBSERVED SPECTRA

Revisiting L95

In L95 the relations between 2D statistics available via observations and the underlying 3D statistics were obtained on the assumption that the observed statistics is determined by density fluctuations. Below we use our results on velocity mapping to interpret power spectra of intensity obtained by Green (1993) in terms of HI density and velocity fluctuations.

Green's observations of the HI emission were accomplished with the Synthesis Telescope of the Dominion Radio Astrophysical Observatory (DRAO) towards $l = 140^\circ, b = 0^\circ$ ($03^h03^m23^s, +58^\circ06'20'$, epoch 1950.0) and they revealed a power law spectrum of 2D intensity. This spectrum is proportional to $P_2(\mathbf{K})|_{\mathcal{L}}$ and its interpretation depends on whether the slicing is thick or thin.

To answer this question we should estimate both λ and $|\mathbf{K}|$. To estimate λ we use a crude estimate of f , namely, we describe ordered motion of atomic hydrogen in the outer parts of the Galaxy by a simple flat rotation curve without any distorting radial motions. In this case the parameter f which describes line-of-sight projection of the shear in a rotational flow is

$$f \approx -\frac{1}{2A} \frac{\sin l}{(\alpha + \sin l)^2 \sqrt{1 - (\alpha + \sin l)^2}} \quad (52)$$

²²Our earlier statement of the possible change of the spectral index can be understood as through this suppression. Indeed, for $\delta V/3.5v_{T(warm)} \ll 1$ the contribution of the warm media is negligible, while it increases with δV .

where $A = 14 \text{ km/s/kpc}$ is the Oort's constant and $\alpha = V_z/V_0$, where $V_0 \approx 220 \text{ km s}^{-1}$ and V_z is the relative velocity of HI parcel. This relative velocity varies from 0 at $z = 0$ to $-V_0 \sin(l)$ for the gas parcel at $z = \infty$. Correspondingly, the parameter f , which is negative, grows in magnitude from the familiar $1/A \sin(2l)$ in the Sun vicinity to larger negative values for distant HI regions. In particular, Green's data covers the velocities V_z up to $\sim -100 \text{ km/s}$, thus f ranges from $-72.5 \text{ pc}/(\text{km/s})$ to $-460 \text{ pc}/(\text{km/s})$.

If we assume that velocity variations at the scale 30 pc amount to 10 km/s and arise from the Kolmogorov turbulence, the structure functions of velocity are

$$D_{LL}(r) \approx 100 \left(\frac{r}{30 \text{ pc}} \right)^{2/3} \text{ km}^2 \text{ s}^{-2} \quad , \quad (53)$$

where the cut-off of the function at large scales is disregarded on the assumption that turbulence is being studied at the scales much less than r_c . Thus λ given by eq. (18) is $\approx 3.5 \text{ kpc}$ for the closest slice and $\approx 56 \text{ kpc}$ for the most distant slice.

The width of the interferometer channels combined to give a single data point in Green's dataset is $\delta V = 5.94 \text{ km/s}$. The slice thickness in parsec is $\mathcal{L} \approx \delta V f \text{ pc}$, and varies from $\approx 600 \text{ pc}$ for the closest slices to $\approx 2200 \text{ pc}$ for the distant ones²³. The wavenumber of transition from *thin* to *thick* slice given by eq. (36) is equal 0.16 pc^{-1} .

Figure 4 shows the range of the scales involved (see Green (1993)). The smallest $|\mathbf{K}|$ span from $\sim 1/3 \text{ pc}^{-1}$ for the closest slices to $1/200 \text{ pc}^{-1}$ for the distant ones²⁴, and therefore $|\mathbf{K}|\lambda \gg 1$. The range of values corresponding to $|\mathbf{K}|^{-1}$ is shown by the darkened region in the plot. If we deal with cold HI, most of them, except the nearest slices correspond to the regime where slice is *thin*. For warm HI the border line is different and most of the scales correspond to *very thick* slice.

We have shown earlier that the contribution of the warm component is suppressed unless the slices are thin for both components. The latter regime corresponds to the parameter space below the line "cold HI" in Fig. 4. For such close slices the actual geometry of the diverging lines of sight must be accounted for (see Lazarian 1994b) and we consider the resulting complications elsewhere. If the intensity contributions of the warm and cold HI are comparable, it is possible to show (see section 4.3) that the cold HI contribution will dominate the spectra above the "cold HI" line.

Our analysis of Figure 4 and Figures 1 and 2 shows that *if the spectrum of density is shallow (i.e. $n > -3$)*, the observations by Green (1993) reveal the spectrum with index $n + m/2$. For $m = 2/3$ the spectrum of emissivity obtained by Green (1993), namely the emissivity with the index ~ -2.7 , corresponds to $n \sim -3$. This conclusion is not sensitive to the values of density correlation scale r_0 (see Eq. (30)), which we estimated to be of order of 20 pc .

If, however, the density spectrum is steep (i.e. $n < -3$), the fluctuations of 21 cm intensity observed by Green (1993) can arise from velocity fluctuations. In this case the spectral index is $-3 + m/2$. For $m = 2/3$ one gets the slope $-8/3 \approx -2.7$ which is exactly what is observed.

In the case of the Galaxy, the steepening of the spectrum depends on the scale $|\mathbf{K}|^{-1}$ as shown in Figure 5. This figure should be not interpreted literally for large \mathcal{L} , however. First of all, when the thickness of the region becomes comparable to the distance to it, one should account for the divergence of lines of sight (Lazarian 1994b). Moreover, our model that assumes infinitely extended media does not hold and effects of finite size of the emitting region become important when \mathcal{L} becomes comparable with the size of the Galactic disk (see Appendix E).

SMC

Small Magelanic Cloud (SMC) is rather irregular galaxy and the Earth observer looks at it from outside.

²³Note, that the cut-off due to thermal velocity (see section 2.1) in Warm Neutral Medium (see table of idealized phases in Draine & Lazarian (1999)) is $\sim 6 \text{ km/s}$. If the WNM constitutes the dominant fraction of the neutral phase (Dickey 1995) then the velocity resolution above is optimal and no further decrease in δV will result in getting new information. However, if close to Galactic plane Cold Neutral Media constitutes a substantial portion of mass, the increase of velocity resolution up to 1 km/s is desirable.

²⁴We stress that our analysis should be modified for the largest scales which are larger than r_c .

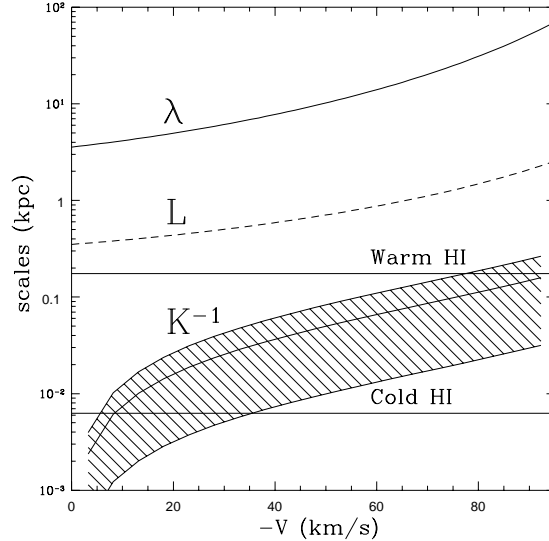


FIG. 4.— The variations of geometric scales with the sampling velocity are shown. The upper curve corresponds to the variations of the correlation scale λ in the velocity space. The middle curve corresponds to the variations of the slice thickness \mathcal{L} . The darkened area in the Figure depicts to the range of the turbulence scales under study in Green (1993). The solid curve within the darkened area corresponds to the interferometric measurements with the baseline 21 m. The lower horizontal line denotes value of $|\mathbf{K}|^{-1}$ which separates *thin* (above) and *thick* slice regimes for cold HI and the upper line denotes a similar value for the warm HI.

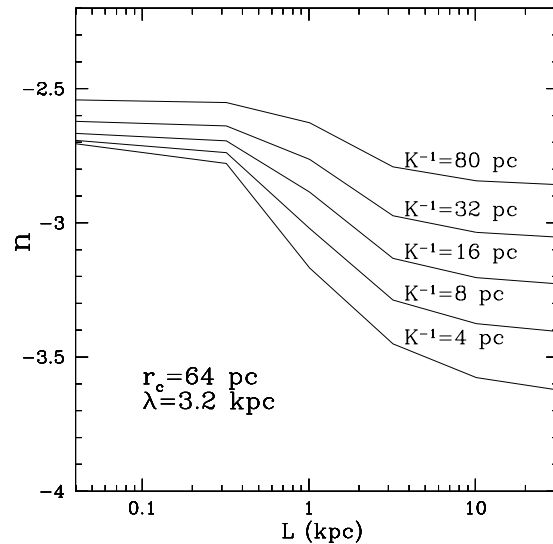


FIG. 5.— The variations of the spectral index n of the 21 cm intensity spectrum with the thickness of the slice \mathcal{L} for the turbulence with Kolmogorov velocity spectrum and long-wave dominated density spectrum. To provide the feelings of the scales involved we expressed our results in parsecs.

For its study the modification of our technique described in the Appendix E is applicable. As the result, the size of the SMC plays the role of the parameter λ and with this modification our earlier formulae are applicable.

An advantage of using SMC is that the effects related to the divergence of lines of sight are negligible for the study and this simplifies the analysis for thick slices. Data on SMC in Stanimirovic et al. (1999), Stanimirovic et al. (2000) and Stanimirovic (private communication) shows that for thin slices the slope is ≈ -2.8 but it steepens up to ≈ -3.4 as the integration over the whole emission line is performed. Note, that in the latter case the intensity fluctuations arise from density fluctuations only and the spectral index of P_2 corresponds to the 3D spectral index of underlying density turbulence. This

means that the density spectrum has an index -3.4 , which is close to the Kolmogorov $-11/3$ index. As this index is less than -3 , the fluctuations should be “velocity-dominant” and the corresponding index should be $-3 + m/2$, provided that the slice is “thin”. The measured spectrum is a bit steeper than in the Galaxy. Is this difference meaningful? Does it mean that the spectrum of turbulence deviates from the Kolmogorov law? Is this a reflection of a transition to thicker slicing? A detailed study of the SMC data should answer these sort of questions. At the current stage it looks to us that there exist a rough agreement between the data and the assumption that both density and velocity spectra have the Kolmogorov index of $-11/3$.

An additional interest to SMC data stems from the fact that variations of the power law may shed light on the nature of turbulence in warm HI. We discussed above that the fluctuations in sufficiently thin slices are dominated by the cold component. As the thickness of slice increases the relative contribution of the warm component increases. The fact that the velocity-integrated data provides the index close to the Kolmogorov one either indicate that the fluctuations of warm HI density are insubstantial or that they have the Kolmogorov index.

Dust and Molecular Data

Dust and HI are well correlated (see Boulanger et al. 1996). Both Galactic and SMC Far Infrared emission exhibits shallow spectrum with the index -3 (Wall & Waller 1998, Waller et al 1998, Stanimirovic et al. 2000). However Stanimirovic et al. 2000 combined data at $100 \mu\text{m}$ and $60 \mu\text{m}$ to show that the actual dust spectrum of dust column density is steeper. In fact the spectrum of dust column density was found has index ≈ -3.6 which is in rough correspondence with the $\approx -3.4 - -3.5$ spectral index for HI (see above). Thus both HI and dust supports the idea that the spectrum of density is steep for diffuse media.

Are there any evidence that that the interstellar density may be shallow? In the theory domain Henriksen (1994) derived a quite shallow spectrum for compressible turbulence, but we do not know whether this result is applicable to HI. Although molecular cloud statistics may be different from that of diffuse HI, comparison of the two is worth doing.

Recently molecular cloud data was discussed in Stutzki et al. (1998). There for both ^{12}CO (data from Heithausen & Thaddeus (1990) and Falgarone et al (1998)) and ^{13}CO (data from Heyer et al. (1997)) transitions the spectrum of intensity was observed to have a power law index ~ -2.8 . As the data is averaged over velocity, the fluctuations of intensity are due to density fluctuations and the spectrum of density should have the same slope as the intensity (i.e. $n = 2.8$, (see Eq. (27)), provided that the transitions are optically *thin*. The trouble is that the lines are optically *thick* and the interpretation above is not applicable. Further research should determine what the particular emissivity index means in terms of underlying statistics of velocity²⁵ and density.

Strangely enough, the shallow spectrum of molecular density fits well in the picture of molecular cloud structure. Stutzki et al 1998 derive the relation²⁶ between the power spectral index n , the spectral index ε of clump mass-size relation $M \propto r^\varepsilon$, and the index \aleph of the clump mass spectrum $dN/dM \propto M^\aleph$:

$$n = (3 - \aleph)\varepsilon$$

$\varepsilon = 2$ corresponds to the Larson’s relations (Larson 1992) and \aleph in the range 1.6 to 1.8 corresponds to the analysis of clumps (Kramer et al. 1998). The trouble is that this relation was derived to be true for optically thin clouds, while the clouds in the analysis by Stutzki et al 1998 are optically thin makes one worried. Further research should concentrate on providing the adequate statistical description for optically thick tracers and comparing the statistics for thin and thick tracers.

6. DISCUSSION

²⁵Although the data is integrated over the emission line, the random velocity is important as self-adsorption depends on the gas velocity dispersion.

²⁶This relation can be applied to individual structures in velocity slices provided that the index of the two dimensional spectrum of intensity fluctuations is used instead of n . In the velocity dominated case the masses would reflect not the masses of the real clumps but caustics produced via projection.

6.1. Our approach

Velocity mapping In the paper thus far we address the problem of the velocity modification of HI statistics. Although the paper deals with HI only, the problem it addresses is quite general and therefore our results are applicable to any optically thin lines. We plan to address the effects of finite optical depth elsewhere.

We showed that intensity fluctuations can arise both from velocity and density fluctuations and derived the 3D spectrum of intensity (eq. (13)) within velocity data cubes. A quick look at eq. (13) shows that the density and velocity enter the expression in a different manner and this eventually enables us to separate the velocity and density contributions.

Statistics used: 2D Spectra

Channel maps and the related 2D spectra constitute the central topic of this study. This is because the channel maps are readily available via single dish observations, while channel map spectra $P_2(\mathbf{K})$ can be directly obtained with an interferometer.

As we discussed in the previous section it is important to determine whether 21 cm intensity fluctuations are due to density or velocity fluctuations. If the density spectrum is long-wave dominated, our results in Figure 2 indicate that HI intensity spectrum does not reflect the underlying HI density statistics. Therefore the spectrum of the density fluctuations may have any value $n < -3$, but this will not alter the intensity fluctuations unless a substantial portion of the 21 cm line is integrated over and the slice become “thick” in accordance with the criterion (36).

Additional statistics: 1D and 3D Spectra

In view of the problems we face with the interpretation of present HI results it is important to make use of other statistical tools. Indeed, 2D statistics of channel maps is not the only statistics that is available. Using data cubes one can obtain the 3D spectrum P_s which properties are described in the Appendix B. Alternatively, an additional insight can be obtained if 1D spectra are formed using velocity cubes. We discuss these new statistical tools in Appendix F and show that 1D spectra is complementary to the tools we employed in the main text. In fact, using this statistics one does not need to change the velocity slice thickness to distinguish between long and short-wave dominated density spectra. If the density field is long-wave dominated we expect to see the power index $-2/m$, while if the density spectrum is short-wave dominated we expect to get the index $2(n+2)/m$. This test can be performed with the existing 21-cm data cubes. For $n = -3$ the predictions for the two cases coincide. Naturally the spectra are not independent, but they are produced using different procedures of data handling and therefore provide an additional test.

6.2. Problems of Interpretation

“Big Power Law”

The application of our technique to the available data (see section 5) testifies that the density spectrum of HI in SMC has a power-law index close to the Kolmogorov value of $-11/3$ over the scales from 40 pc to 4 kpc. Assuming that density statistics in our Galaxy is steep (as in SMC) we also get that the velocity has an index of $\sim -11/3$ from 10 to 100 pc. The proximity of indexes for both velocity and density spectra to the Kolmogorov values is both remarkable and unexpected. First of all, there are good reasons why we should not *a priori* expect to find Kolmogorov-type turbulence in interstellar medium (Lazarian 1999a). Moreover, Kolmogorov interpretation would entail problems with understanding of the nature of energy injection. We also noted earlier that SMC possibly shows a density spectrum with only marginal velocity contribution, which would mean that the structures we observed are static. The last point requires a further investigation, however.

It is very strange, but Astrophysical turbulence whenever it is measured seem to exhibit Kolmogorov power slope. The existence of the “Big Power Law” (see Armstrong et al 1995, Spangler 1999) is one of the great Astrophysical mysteries. Measurements of turbulence in ionized media established a spectrum with $-11/3$ index at the scales from a few AU to a fraction of a parsec. Measurements at larger scales are much less reliable (Cordes 1999) and although compatible with the $-11/3$ index allow other interpretations. Contrary to our intentions (see L95, Lazarian 1999a) we contributed to making

the problem even less tolerable. It looks now that the “Big Power Law” spreads up to scales of several kpc.

MHD turbulence

Ignoring for the moment the issue of energy injection scale and associated problems we may ask whether we expect to see the turbulence with the index close to the Kolmogorov one when the fluid is strongly magnetized.

The Kolmogorov-type spectrum of plasma density fluctuations observed via radio scintillations and scattering (see Armstrong et al 1995 and references therein) has been interpreted recently as the consequence of a new type of MHD cascade by Goldreich & Sridhar (1995). The Goldreich-Shridhar model of turbulence²⁷ differs considerably from the Kraichnan one (Iroshnikov 1963, Kraichnan 1964). It accounts for the fact that hydrodynamic motions can easily mix up magnetic field lines in the plane perpendicular to the direction of the mean field. Such motions provide eddies elongated along the field direction and the velocity spectrum close to the Kolmogorov one.

The Goldreich-Shridhar turbulence is anisotropic with eddies stretched along magnetic field direction. The wavevector component parallel to magnetic field k_{\parallel} scales as $k_{\perp}^{2/3}$, where k_{\perp} is a wavevector component perpendicular to the magnetic field. Thus the degree of anisotropy increases with the decrease of the scale. The fact that during the observations various scales contribute to the correlation functions of intensity (see discussion in L95) and the contribution of the largest scales dominates the signal mitigate the anisotropy of the intensity statistics. The component of magnetic field parallel to the line of sight decreases anisotropy as well. Indeed, it is easy to see that only the component of magnetic field that is in the plane of the sky will create the anisotropy, while the component of magnetic field parallel to the line of sight “mix up” parallel and perpendicular direction²⁸. Therefore the anisotropy of the 21-cm statistics may not be easy observable (see Green 1994). In our future papers we plan to discuss the observational tests of the Goldreich-Shridhar picture for HI. A simultaneous use of other techniques of turbulence study (see Lazarian 1992, Lazarian 1993) should allow to have a more comprehensive picture of MHD turbulence.

Incompressibility is assumed within the Goldreich-Shridhar picture of turbulence. In actual ISM turbulence the compressibility may be important in view of the fact that the media may be pliable to compressive forces (soft equation of state). It is unclear how the picture of MHD cascade will be changed in this case.

When magnetic field is intermittent, one may expect the thermal instability to be more efficient in the regions with a smaller value of magnetic field. Indeed, if various regions of magnetized gas are at pressure equilibrium, the gas pressure within the regions with lower magnetic field will be higher. This shall increase the density of gas and may initiate thermal instability. Indeed, the heating of gas is proportional to the gas density, while cooling is proportional to the (density)². As the result dense gas will tend to cool down further increasing its density (Spitzer, 1978) making regions with lower magnetic field colder and denser. This would qualitatively correspond to the picture of magnetic measurements in HI by Carl Heiles (private communication). We will quantify the picture and its implications on the small scale structure of HI elsewhere.

Superbubbles and Supershells

One may speculate that the observed statistics is the result of the superbubbles and supershells. Indeed, potentially superbubbles may inject energy on the kpc scale. The issue in this case is why we do not see “knees” in the spectra at the intermediate scales when singular shells inject energy. Does this mean that the supershells should carry an overwhelming amount of energy or the available resolution is not sufficient to see peculiarities related to more localized energy injection?

In general, energy injection scale is critical for understanding interstellar turbulence. For decades it was generally believed that MHD turbulence damps slowly (Iroshnikov 1963, Kraichnan 1964). In this situation supersonically broadened linewidths of molecular clouds could be explained as locally

²⁷A qualitative discussion of the model and the role of reconnection for the cascade can be found in Lazarian & Vishniac (1999).

²⁸No anisotropy is expected for the intensity correlations if the total magnetic field is parallel to the line of sight.

generated, e.g. due to a cloud collapse. However, new understanding of MHD turbulence (Goldreich & Shridhar 1995) and numerical simulations (e.g. Vazquez-Semadeni 1999) suggest that the turbulent damping in magnetized media takes place on the scale of an eddy²⁹ turnover (similar to the case of unmagnetized media). Therefore to allow starless cores to have linewidths similar to those of star-forming cores (Benson & Myers 1989) the energy injection should happen on the scale much larger than the cloud size (for larger eddies the timescale of turnover is larger). Nevertheless, scales of the order of several kpc look excessively large.

Energy injection to molecular clouds may arise directly from shocks (Scalo & Kornreich 1999), and this also can be classified as injection from large scales. The spectrum of shocks is steep ($\sim k^{-4}$) and does not correspond to the observations.

One has to accept that power spectra may be rather rough statistical tools and the index $-11/3$ may have nothing to do with a cascade. For instance, such a density spectrum may emerge in a media with HI shells having a distribution $P(x) \sim x^{8/3}dx$. However, the particular power law does not seem to have particular physical explanation and moreover, small shells are expected to have larger velocities which does not correspond to the observed velocity spectrum.

6.3. Model assumptions and future work

This work is the first, as far as we know, that treats quantitatively fluctuations arising from turbulent velocities. It is not surprising therefore that there are many issues to be studied in depth in the future.

Density-Velocity Correlations

Our derivations above assumed that the turbulent velocity and density are not correlated in Galactic coordinates. This seems to be true at large scales, but may fail on small scales where self gravity may contract HI structures³⁰. Such a correlation may enhance the amplitude of fluctuations observed if the local divergence of the velocity field is negative in the regions of density enhancement (i.e there is systematic inflow of matter into overdense regions) and, *vice versa*, would decrease the amplitude of fluctuations if overdense regions are associated with outflows. However, interstellar medium is far from being quiescent even on the small scales and the sense of velocity-density correlation is unclear for the ISM turbulence. It is easy to see from the equation of continuity that the logarithmic time derivative of density equal to the divergence of the velocity field. This means, that the instantaneous density itself depends on the integral of the velocity divergence and in the complex medium with sequential expansions and collapses the importance of this correlation is difficult to estimate. In any case, we do not expect *a priori* any strong velocity-density correlations.

To check whether the assumption about density-velocity correlation is important for our final results one needs either to do numerical simulations or to assume the statistics for joint density-velocity distribution. In Appendix D we check our results assuming Lognormal distribution for random density³¹ and the velocity and logarithm of density are correlated Gaussian fields.

To estimate the upper limit of the effect of density-velocity correlation we assume the maximal possible value of this correlation. Naturally, in all realistic situations we expect the value of this correlation to be much smaller than this maximal value. Our results for this worst possible regime can be summarized as follows. The criterion for the slice to be thick is increased at most by a factor of a few and all our findings for the thick³² slices (see Table 1) hold. The correspondence between our earlier results and “extremely correlated” results holds for the thin slices in the long-wave regime, which is favored by our analysis of data. For thin slices and short-wave dominated density field (shallow density spectrum) the correlations are shown to enhance the velocity effects. In fact, in the extreme regime of correlations it is velocity, rather than density that dominates the expected channel emissivity. However, we stress that we used

²⁹It is shown in Lazarian & Vishniac (1999) that MHD turbulence allows equivalent descriptions via wave-wave, wave-eddy and eddy-eddy interactions.

³⁰Whether this important in practical terms of HI studies is unclear, as a transition to higher densities entails a transition to molecular hydrogen.

³¹Lognormal distributions naturally arise in numerical simulations of isothermal gas (see Vazquez-Semadeni & Passot 1999).

³²This includes both long-wave and short-wave density field.

an upper limit for these correlations and for interstellar data sets we expect to observe density effects. Changes of the spectrum within the thin slice regime when the density is short-wave dominated can be a signature of strong velocity-density correlations. Using the thick slices it is possible to check whether the density is short-wave or long-wave dominated. A more detailed study of the regime of velocity-density correlations can be done using our expressions in Appendix E and substituting a different law of velocity-density correlations (rather than taking its maximal value), but this study is beyond the scope of the present paper.

Anisotropy and Linear Expansion

It is both challenging and important to determine the degree of the HI spectrum anisotropy and its variation from slice to slice. This information can provide an insight to the nature of HI turbulence and may be used as a diagnostic for the interstellar magnetic field. For instance, measuring the structure functions of HI intensity as a function of a positional angle in an analogy with the statistical treatment of synchrotron fluctuations (see Lazarian 1992) may reveal magnetic field direction in various portions of the sky, provided that the turbulence is indeed Goldreich-Shridhar type. So far, the attempts to measure anisotropy in HI are limited to the Green (1994) study, where no anisotropy was detected. Apparently a better analysis is needed. For the slices with high degree of anisotropy our statistical technique should be modified as suggested in L95.

Another issue is related to the linear expansion (2). If the slice is sufficiently thick the map becomes non-linear. Potentially, knowing a detailed Galactic rotation curve one can describe a non-linear mapping. We found, however, that the linear mapping is OK for both thin and thick regime if we study sufficiently small scales (see discussion after eq. (1)). We also found that if \mathcal{L} is smaller than the distance to the slice, it is possible to ignore the complication related to the radial nature of lines of sight. Thus the theory at its present stage is widely applicable.

Applicability of the theory

The theory presented in the paper is quite general. The mathematical machinery developed here can be used for studying turbulence in various emission/adsorption lines. For instance, velocity effects and line of sight integration are the problems that are also encountered in studies of turbulence inside molecular cloud. Unfortunately, there are additional complications related to studying molecular clouds. For instance, these studies face problems with samples being not statistically homogeneous (see Miesch & Bally 1994). Indeed, it is widely believed that for individual molecular complexes the statistics (especially at large separations) is dominated by regular gradients rather than the random component. To eliminate the inhomogeneous component Zurfluh (1967) or other types of spatial filtering (see Spicker & Feitzinger 1988a,b) can be used. However, Stutzki et al (1998) have shown that the statistics can be obtained without such filtering if the particular modification of wavelet analysis, namely, so-called Alan variances are used. For power-law statistics Stutzki et al. (1998) relate their statistical measures to the spectrum and correlation functions that are used in the present study. Therefore the translation of our results to the language of Alan-variables is trivial.

What is less trivial is to account for the finite optical depth effects for particular emission lines. In treating this problem the adsorption by dust presents the least of the evils. We expect more complex dependences treating self adsorption within an emission line. The optical thickness in this case will depend on the velocity adsorption.

Our present results are obtained for 21 cm emission transitions which intensity is proportional to the integrated density of HI along the line of sight. Other emissivities, e.g. those of H_α lines are proportional to the squared density of species. It is possible to generalize our results for those transitions and contribute to the studies of ionized emitting media, e.g. of HII regions (O'Dell 1986, O'Dell & Castaneda 1987).

Other generalizations are also straightforward. Our present research was motivated primarily by the necessity to interpret the existing interferometric data and therefore in the paper we mostly dealt with spectra. As the result, correlation functions (see Appendix C) serve auxiliary purposes in our study. With other sets of data, correlation functions may be more advantageous and our analysis of their properties in Appendix C is useful. Moreover, modifying our technique it is possible to study various moments of the line-shape (Lazarian 1992), e.g. velocity centroids (see Dickman 1985). In our future

paper we shall discuss all these possibilities.

HI data and simulations

In the paper we predicted how the power slope will change with the thickness of the velocity slice as a function of velocity and density statistics and the ratio of the cold and warm HI filling factor. It is important to test these our predictions against observations. The SMC data is an example of the data set that can be used for the purpose.

It is also important to verify our ideas using simulations. Our results on velocity and density correlation were tested so far only for Lognormal distribution where we managed to get an analytical result. Using the statistics that arises from simulations is on the agenda. We would stress that the only 3D simulations are useful. Due to a limited dynamical range these simulations do not show power-law behavior and additional care is required for comparing these results with our predictions.

Clouds and Filaments

HI data cubes, exhibit a lot of small scale emissivity structure³³. The question is what part of them is real, i.e. is associated with density enhancements in galactic coordinates and what part of them is produced by velocity fluctuations. A related question is whether the structures we see are produced dynamically, through forces, e.g. self-gravity, acting on the media or they may be produced statistically exhibiting the properties of random field. The second question was partially answered in Lazarian & Pogosyan (1997), where it was shown that density fluctuations with Gaussian distribution and power spectra result in filamentary structures. The structures become anisotropic and directed towards the observer when the velocity effects are accounted for.

The issue of density enhancements produced by velocity fluctuations is closely related to the statistics of “clouds” observed in velocity space. The results on velocity mapping that we discussed earlier suggest that spectra of fluctuations observed in velocity slices are more shallow than the underlying spectra. This means more power on small scales or, in other words, more small scale structure (“clouds”) appears in the velocity slices due to velocity fluctuations. Understanding of the velocity mapping may help to solve the problem of discrepancy between counts of clouds observed in emission and extinction (compare Scalo & Lazarian 1996).

The integrated velocity maps are sensitive to density fluctuations and may provide means of solving the problems of the statistics of actual density inhomogeneities.

Beyond 2-point Statistics

Is the power spectrum the best one can get? Power spectrum does not reflect the clustering properties of the medium. To find those characteristics one should use multi point statistics, of which the simplest would be the so-called bi-spectrum (Scoccimarro 1997). This type of statistics is sensitive to clustering properties of the media and we may hope to relate the bi-spectrum with the inflows observed in molecular clouds (see Myers & Lazarian 1998) and the processes of star formation. Other potentially useful tools, e.g. genus analysis are discussed in Lazarian (1999b). A choice of a particular tool depends on the sort of questions one attempts to answer. This paper is limited to making use of channel map spectra.

All in all, we believe that the machinery developed in the present paper opens avenues for both theoretical and observational research and the appropriate studies should contribute to unraveling the mystery of ISM turbulence. At the same time a search for new statistical tools appropriate for diagnostic of ISM turbulence should continue.

7. CONCLUSIONS

The results of the present work can be summarized as follows:

1. The emissivity spectrum arises both from velocity and density fluctuations. The emissivity statistics depends on the thickness of the velocity slice. The minimal value of the effective thickness depends on the temperature of the gas. We found limiting regimes that we termed “thick” and “thin” velocity slices (for criteria see Eq. (35)) and obtained asymptotics for these regimes. Thermal velocity acts to increase the effective thickness of the slice without increasing the amplitude of the signal. For a mixture of cold and warm HI the slice may be thin for cold phase and thick for the warm phase. In this case the the

³³It was noticed by Langer, Wilson & Anderson (1993) that more structure is seen in spectral line data cubes than in the integrated intensity maps.

expected relative contribution of warm medium is suppressed.

2. Two dimensional spectrum of 21 cm intensity (that can be measured by interferometer) corresponds to the integral of the underlying 3D spectrum if the slicing is thin while in the thick slice regime the result depends on whether the density is short- or long-wave dominated (see below for the criterium definition). The 3D spectrum is anisotropic and can be expressed through the velocity and density statistics.

3. For Galactic data we find that the slice is thick if the two dimensional wavenumber $|\mathbf{K}| > (\delta V^2/C)^{1/m} \approx 0.16 \text{ pc}^{-1}$, which means that the present day radiointerferometers provide a thin slicing of Galactic disk data. Density and velocity enter our formulae in a non-symmetric fashion. Therefore the slope of the HI emissivity spectrum changes with the thickness of the slice and this allows to find the slopes of the spectra of velocity and density fluctuations separately.

4. For thin slices the velocity fluctuations make spectra of emissivity more shallow creating a lot of structures in PPV space that can be erroneously identified as clouds. For long-wave dominated density most of the small scale structures are due to velocity fluctuations both in thin and thick slice regimes.

5. If the overdensity is dominated by small scale inhomogeneities (i.e. the correlation functions scale as $1/r^\gamma$, $\gamma > 0$), the statistics of the channel maps is dominated by density fluctuations. The HI observational data seem not to support shallow density spectrum, however.

6. If the overdensity is dominated by large scale fluctuations (i.e. the structure functions scale as $1/r^\gamma$, $\gamma < 0$), the statistics of the channel maps is dominated by velocity fluctuations. In this case, to measure density one should use *very* thick slicing $\mathcal{L} \gg \lambda$, where λ is given by Eq. (18). In thin slices one will find universal 2D spectral slope $\approx -8/3$ if velocity field is described by the Kolmogorov index $m = 2/3$. Data on the galactic HI statistics and that of SMC roughly agree with this spectrum.

7. The two cases above (i.e. $\gamma > 0$ and $\gamma < 0$) can be distinguished by varying the thickness of the velocity slice. The analysis of the observational data suggests that the HI density spectrum has an index close to the Kolmogorov one, namely, $-11/3$ and the statistics of the velocity field is also Kolmogorov-type. Thus one may argue that the observed emissivity spectrum might be a signature of the Goldreich-Shridhar (1995) MHD turbulence. The developed mathematical machinery is applicable to studies of turbulence both in Galactic disc and individual clouds (see Appendix E). Various emission lines can be used and the technique can be modified to account for finite optical depth effects.

The authors are grateful to Roman Scoccamarro for sharing his results before publication and numerous useful discussions. The presentation of the material has been improved following very helpful comments by John Scalo. Discussions with Robert Brawn, Snezana Stanimirovic and Steve Shore during the ‘‘Cosmic Evolution and Galaxy Formation’’ conference, Puebla, Mexico were helpful at the final stage of our work and we would like to thank Jose Franco for inviting us. We would like to thank Nick Kaiser for illuminating exchanges. AL is grateful to Jay Gallagher, Linda Spark whose suggestions helped to improve the presentation of the material. A.L. also acknowledges NASA grant NAG5 2858 and valuable suggestions by Chris McKee.

APPENDIX

LIST OF NUMERICAL CONSTANTS

Relevant to Table B2

3D power spectrum

$$a_n = 2\pi^2\Gamma(-n)/\left|\Gamma\left(\frac{3+n}{2}\right)\right|\Gamma\left(\frac{1-n}{2}\right) \quad \text{eq. (E10)}$$

$$b_m = \frac{m}{12}\pi^2\Gamma(5+m)/\Gamma(1-m/2)\Gamma(3+m/2) \quad \text{eq. (B7)}$$

m/n	-1	-5/3	-2	-3	
1/2	74.8279	434.657	1361.75	84244.6	eq. (B10)
2/3	35.4366	88.5916	172.584	2205.93	
1	19.1096	23.0004	29.4949	92.5001	

where the numbers at the right hand side correspond to the formulae in Appendix B where the constants appear first.

Relevant to Table 1 and Table C3

2D power spectrum,

$$A_n = a_n$$

$$B_m = (13/5\pi) b_m$$

$$S_{nm} = 2^{-n-(m+1)/2} \pi \Gamma\left(-\frac{2n+m}{4}\right) / \left| \Gamma\left(\frac{3+n+m/2}{2}\right) \right|$$

Correlation function,

$$c_{\gamma m} = 2^{(\gamma+m-1)/m} \Gamma\left(\frac{2\gamma+m-2}{2m}\right) / m\pi^{\frac{1}{2}}$$

$$C_{\gamma m} = \Gamma\left(\frac{2\gamma+m-2}{4}\right) / 2^{\frac{1}{2}} \Gamma\left(\frac{2\gamma+m}{4}\right)$$

ASYMPTOTICS AND SPECIAL REGIMES FOR 3D POWER SPECTRUM

We discuss asymptotics and introduce useful approximations of the integrals involved in computation of the 3D power spectrum $P_s(\mathbf{k}) = P_\rho(\mathbf{k}) + P_v(\mathbf{k})$. If the density correlation function is given by eq. (30) Introducing new dimensionless variables

$$y = kr \tag{B1}$$

$$x = \cos \theta$$

$$\phi = (k\lambda)^{2-m} \mu^2 = \lambda^{2-m} k_z^2 k^{-m} \quad ,$$

we can present the 3D spectrum $P_s(\mathbf{k})$ (see eq. (16)) as

$$P_s(\mathbf{k}) = P_v(\mathbf{k}) + P_\rho(\mathbf{k}) \quad , \tag{B2}$$

$$P_v(\mathbf{k}) = k^{-3} \mathcal{I}_3(\mu, \phi) \quad ,$$

$$P_\rho(\mathbf{k}) = k^{\gamma-3} r_0^\gamma \mathcal{I}_{-n}(\mu, \phi) \quad .$$

$$\mathcal{I}_\alpha(\mu, \phi) = 2\pi \int_0^\infty y^{\alpha-1} dy \int_{-1}^1 dx J_0\left(y\sqrt{(1-\mu^2)(1-x^2)}\right) \cos(y\mu x) e^{-\phi y^m(2+m(1-x^2))/4} \quad , \tag{B3}$$

where $\alpha = 3$ or $-n$ and J_0 is the Bessel function of the zeroth order. We have to calculate P_v and P_ρ in another combination when the density correlation function is given by eq. (47)

It is most illuminating to start by expanding the plane wave in the eq. (13) into multipoles

$$e^{i\mathbf{k}\cdot\mathbf{r}} = 4\pi \sum_{\text{lm}} i^l j_l(kr) Y_{\text{lm}}(\hat{\mathbf{k}}) Y_{\text{lm}}^*(\hat{\mathbf{r}}) \quad , \tag{B4}$$

where $j_l(kr)$ is a spherical Bessel function and Y_{lm} are spherical harmonics. After performing trivial integration over the polar angle in eq. (13) and making the dy integration the innermost one we get

$$\mathcal{I}_\alpha(\mathbf{k}) = 8\pi^2 \sum_1 (i^l) Y_{10}(\mu) \int_{-1}^1 dx Y_{10}^*(x) \left(\int_0^\infty y^{\alpha-1} dy j_1(y) e^{-\phi y^m(2+m(1-x^2))/4} \right) \tag{B5}$$

In this Appendix we consider two asymptotics, one ‘‘long-wave’’ corresponding to small ϕ and the ‘‘short-wave’’ corresponding to large ϕ . In the long-wave limit ϕ (see eq. (B2)) tends to zero and the integration is trivial. In this case \mathcal{I}_α is just a constant which coincides with the value of \mathcal{I}_α in the absence of random velocity

$$\mathcal{I}_\alpha(\mu, 0) = 2\pi^2 \frac{\Gamma(\alpha)}{\Gamma\left(\frac{3-\alpha}{2}\right) \Gamma\left(\frac{1+\alpha}{2}\right)} \quad . \tag{B6}$$

The result is the same if one considers the wave modes orthogonal to the line of sight ($\mu = 0$) which are unaffected by velocity mapping $\mathcal{I}_\alpha(0, \phi) = \mathcal{I}_\alpha(\mu, 0)$.

For the term P_ρ arising from density perturbations $\alpha = -n < 3$ and $\mathcal{I}_{-n}(\mu, 0)$ is finite. For the velocity term P_v , $\alpha = 3$ and eq.(E10) gives zero value. The δ -function at $k = 0$ which is contained in P_v and describes the mean density in velocity space has been implicitly omitted by the choice of a variable y . To get more informative result, we expand eq. (B5) up to terms with ϕ to the first power, and after integration over angles obtain

$$\mathcal{I}_3(\mu, \phi \rightarrow 0) \approx b_m \left[1 + \frac{3}{5} \left(\frac{1}{2} - \mu^2 \right) \right] \cdot \phi, \quad (\text{B7})$$

where

$$b_m = \frac{m}{12} \pi^2 \frac{\Gamma(5+m)}{\Gamma(1-m/2)\Gamma(3+m/2)}. \quad (\text{B8})$$

Note, when we expand the exponent in powers of ϕ each next term of the expansion subsequently gives rise to higher multipoles in l series. Namely, the zeroth-order term in ϕ leads only to a monopole contribution, the first-order terms add quadrupole, the second-order add an octupole etc.

Let us derive the short-wave asymptotics for eq. (B5). We note that the function $j_1(y)$ is peaked, roughly, at $y = 1 + 1/2$, so if the exponential cut-off occurs at lower y , the corresponding l -term can be neglected. Thus only low multipoles remain in the sum for large ϕ . Indeed, for a given ϕ high multipoles $l + \frac{1}{2} > \left(\frac{3+m}{6} \phi \right)^{-1/m}$ give vanishing contribution into eq.(B5). Here we use an estimate for the average value of the angle $\langle x^2 \rangle = 1/3$ to get $(2 + m - m \langle x^2 \rangle)/4 = \frac{3+m}{6}$.

Short-wave (i.e. high ϕ) asymptotics follows when only monopole is left in the multipole expansion (B5). This is valid, formally, when $l = 2$ quadrupole is cut out (since the integrals of a dipole is zero). The criterion for this is $\phi > \frac{6}{3+m} \left(\frac{2}{5} \right)^m \approx 1$. Therefore

$$\mathcal{I}_\alpha(\mu, \phi > 1) \approx 2\pi \int_0^\infty y^{\alpha-1} dy j_0(y) \int_{-1}^1 dx e^{-\phi y^m (2+m(1-x^2))/4} \quad (\text{B9})$$

For very short waves, i.e. $\phi \gg 1$ one can put $j_0(y) = 1$ in eq.(B9) to obtain the limit

$$\mathcal{I}_\alpha(\mu, \phi \rightarrow \infty) \rightarrow \left[\frac{8\pi}{m} \left(\frac{4}{m+2} \right)^{\frac{\alpha}{m}} \int_0^\infty y^{\frac{2\alpha-m}{m}} e^{-y^2} D \left(y \sqrt{\frac{m}{m+2}} \right) \right] \phi^{-\frac{\alpha}{m}} \quad (\text{B10})$$

$D(y)$ is the Dawson integral. The factor in brackets, s_{nm} , is tabulated in Appendix A.

We found that eq. (B9) well approximates expression (B5) for all ϕ . Indeed, both long-wave asymptotics eq. (B6) and the short-wave asymptotics eq. (B9) are obtained with only $l = 0$ term in eq. (B5). We checked numerically that eq.(B9) provides an accurate approximation for \mathcal{I}_{-n} , $n \neq -3$, for all values of μ and ϕ . This is a very welcomed simplification, since eq. (B9) depends on ϕ rather than on k and μ separately. For $\alpha = 3$ at small ϕ the zeroth-order μ -independent term (B6) is equal to zero and the in linear ϕ term of \mathcal{I}_3 at low ϕ has the μ -dependent amplitude (see B7). In this case Eq. (B9) provides an angle-average estimate.

The deviation of the expression (B9) from (B5) is less than 3% for $\alpha = 1$. In fact, we found the following formula to be even more accurate numerically while still depending only on ϕ variable

$$\mathcal{I}_\alpha(1, \phi) = 2\pi \int_0^\infty y^{\alpha-1} dy \int_{-1}^1 dx \cos(yx) e^{-\phi y^m (2+m(1-x^2))/4} \quad (\text{B11})$$

This expression is exact for the modes parallel to the line of sight ($\mu = 1$) with $\phi = (k\lambda)^{2-m}$. Being extended to general $\phi = (k\lambda)^{2-m} \mu^2$ it gives an excellent approximation to the full result.

Above we discussed the asymptotics of the integral (B3) that can be found analytically. The Table B2 summarizes our results for the power spectrum in the velocity space. In velocity space the spectrum

	$(k_z\lambda)^2 \ll (k\lambda)^m$	$(k_z\lambda)^2 \gg (k\lambda)^m$
$\lambda^{-3}P_\rho(\mathbf{K}, k_z) :$	$a_n(r_0/\lambda)^{n+3} \cdot (k\lambda)^n$	$s_{nm}(r_0/\lambda)^{n+3} \cdot (k_z\lambda)^{2n/m}$
$\lambda^{-3}P_v(\mathbf{K}, k_z) :$	$b_m \left[1 + \frac{3}{5}(1/2 - k_z^2/k^2)\right] \cdot (k_z\lambda)^2/(k\lambda)^{3+m}$	$s_{-3m} \cdot (k_z\lambda)^{-6/m}$

TABLE B2

ASYMPTOTICAL BEHAVIOR OF THE 3D SPECTRUM IN VELOCITY SPACE. NUMERICAL CONSTANTS a_n, b_m AND s_{nm} ARE GIVEN IN APPENDIX A.

is anisotropic, depending separately on 2D wavevector \mathbf{K} , perpendicular to the line of site and k_z component, parallel to the line of site, $k^2 = |\mathbf{K}|^2 + k_z^2$.

The first (“long-wave”) asymptotics is achieved for waves longer than a velocity correlation scale λ or for the waves transverse to the line of sight, which are unaffected by velocity mapping. The second (“short-wave”) asymptotics is reached for waves that are shorter than the turbulence length *and* have non-negligible component in z-direction.

In Fig. B6 and Fig. B7 we show results of numerical calculations for the total spectrum in velocity space $P_s = P_\rho + P_v$ obtained for $r_0 = \lambda$ and $r_0 = 0.02\lambda$ respectively. In the former case the transition for the short-wave asymptotics happens exactly at the same scale as density correlation scale, while in the latter, more realistic case the velocity scale significantly exceeds density correlation scale. Naturally, when density in Galactic coordinates is less correlated the caustics caused by velocity fluctuations become important. The comparison of Fig. 5 and Fig. 6 confirms this tendency. The results for P_v and P_ρ constitute the basis for our computation of 2D spectra in the main text and 1D spectra in Appendix F.

3D CORRELATION FUNCTIONS

The two-point correlation function is an alternative to a power-spectrum description of the density field. In the velocity space the correlation function $\xi_s(\mathbf{R}, z)$ is obtained by the inverse Fourier transformation of the spectrum $P_s(\mathbf{k})$, $\xi_s(\mathbf{R}, z) = (2\pi)^{-3} \int d^3\mathbf{k} e^{-i\mathbf{k}\cdot\mathbf{r}_s} P_s(\mathbf{k})$. Here, as in the main text, we use capital letters to denote vectors perpendicular to the line of sight and therefore the total vector in the velocity space is $\mathbf{r}_s = (\mathbf{R}, z_s)$ and $R \equiv |\mathbf{R}|$. With an anisotropic $P_s(\mathbf{K}, k_z)$ given by (13), the integration over \mathbf{K} in eq. (21) leads to delta function, which can be used to eliminate the integral over \mathbf{R} . The integral over k_z in eq. (21) can be done analytically to obtain

$$\xi_s(R, z_s) = \int dz \xi(R, z) \left[\left(2\pi\lambda^2 \tilde{D}_z(R, z) \right)^{-\frac{1}{2}} \exp \left(-\frac{(z_s - z)^2}{2\lambda^2 \tilde{D}_z(R, z)} \right) \right] \quad (\text{C1})$$

Here $\tilde{D}_z(R, z)$ describes a velocity structure tensor, i.e. $\tilde{D}_z(R, z) = (r/\lambda)^m \left[1 + \frac{m}{2}(1 - z^2/r^2) \right]$ in the case of solenoidal turbulence, and $r^2 = \mathbf{R}^2 + z^2$. In the absence of the random velocity field $\lambda \rightarrow 0$ the kernel in the brackets transforms to a delta function $\delta(z_s - z)$, and, as one expects $\xi_s(R, z_s) \rightarrow \xi(r)$. Similarly to the split of power spectrum, the correlation function can be split in two parts $\xi_s = 1 + \xi_v + \xi_\rho$, where unity describes mean density in velocity space, ξ_v comes from the random velocity map of the mean density term and corresponds to the first integral in (C1) minus unity, while ξ_ρ arises from the transformation of the underlying correlations of density perturbations $\xi(r)$. It is useful to introduce dimensionless variables $\tilde{r}, \tilde{\mathbf{R}}, \tilde{z}$ which measure distances in terms of the velocity correlation scale λ , i.e

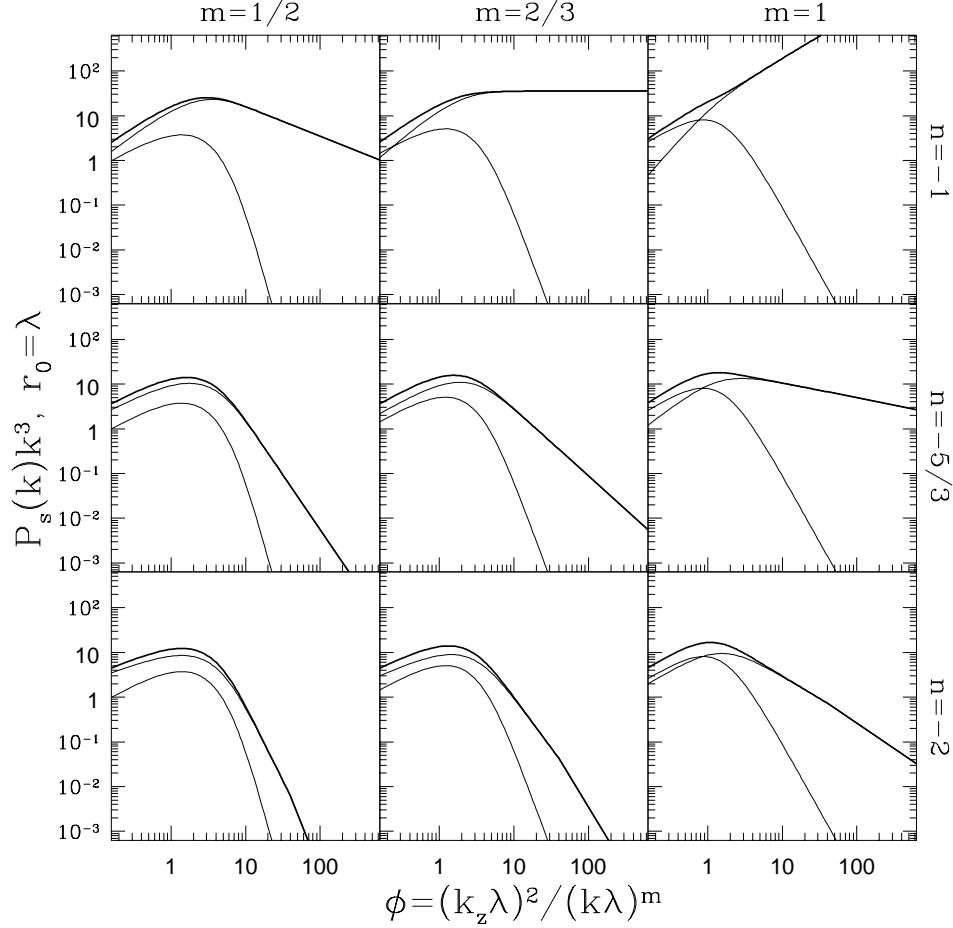


FIG. B6.— The quantity $P(k)k^3$ for various values of m and $n = \gamma - 3$; $r_0 = \lambda$. The short wave part of the spectrum is the function of the variable $\phi = (k_z \lambda)^2 / (k \lambda)^m$ only. Although the longwave spectrum depends separately on k_z and k , we have shown the total spectrum in ϕ variable, assuming the modes to be along the line of sight $k_z \sim k$. In each plot the heavy line shows the total spectrum $P_s = P_\rho + P_v$, while two light lines show P_ρ and P_v terms separately. The term originated from the underlying density perturbations P_ρ dominates at large wavenumbers.

$\tilde{r} = r/\lambda$, etc. Then, with $\gamma = 3 + n$ denoting a slope of the correlation function $\xi(r)$

$$\xi_v(\tilde{R}, \tilde{z}_s) = -1 + \int d\tilde{z} G(\tilde{R}, \tilde{z}_s, \tilde{z}) \quad (\text{C2})$$

$$\xi_\rho(\tilde{R}, \tilde{z}_s) = (r_0/\lambda)^\gamma \int d\tilde{z} (\tilde{R}^2 + \tilde{z}^2)^{-\frac{\gamma}{2}} G(\tilde{R}, \tilde{z}_s, \tilde{z}) \quad (\text{C3})$$

$$G(\tilde{R}, \tilde{z}_s, \tilde{z}) = (2\pi \tilde{D}_z(\tilde{R}, \tilde{z}))^{-\frac{1}{2}} \exp\left(-\frac{(\tilde{z}_s - \tilde{z})^2}{2\tilde{D}_z(\tilde{R}, \tilde{z})}\right) \quad (\text{C4})$$

Two specific cases are of particular interest, namely, 2D correlation function in a slice of fixed velocity $\xi_s(R, 0)$ and 1D correlation along the line of sight $\xi_s(0, z_s)$. The first one corresponds to 2D correlation function measured in a *thin* slice. Asymptotical behavior of $\xi_s(R, z_s)$ is given in Table C3.

The asymptotical formulae for ξ_ρ are valid for $\gamma + m/2 > 1$. As it should be, the correlation function is unchanged by velocity map at large separations, having the same slope γ as the underlying $\xi(r)$. If $\gamma > 1$, the slope of correlation function at small separations is changed, becoming more shallow $-\gamma + (1 - m/2)$ for correlation in the slice of fixed velocity, but steeper $-\gamma - \frac{(2-m)}{m}(\gamma - 1)$ for the correlation along the line of sight, if $\gamma > 1$. Interestingly, for $\gamma = 1$ there is no change of correlation slope along the line of sight. However the amplitude of correlation at small distances is enhanced by the factor $1/m$.

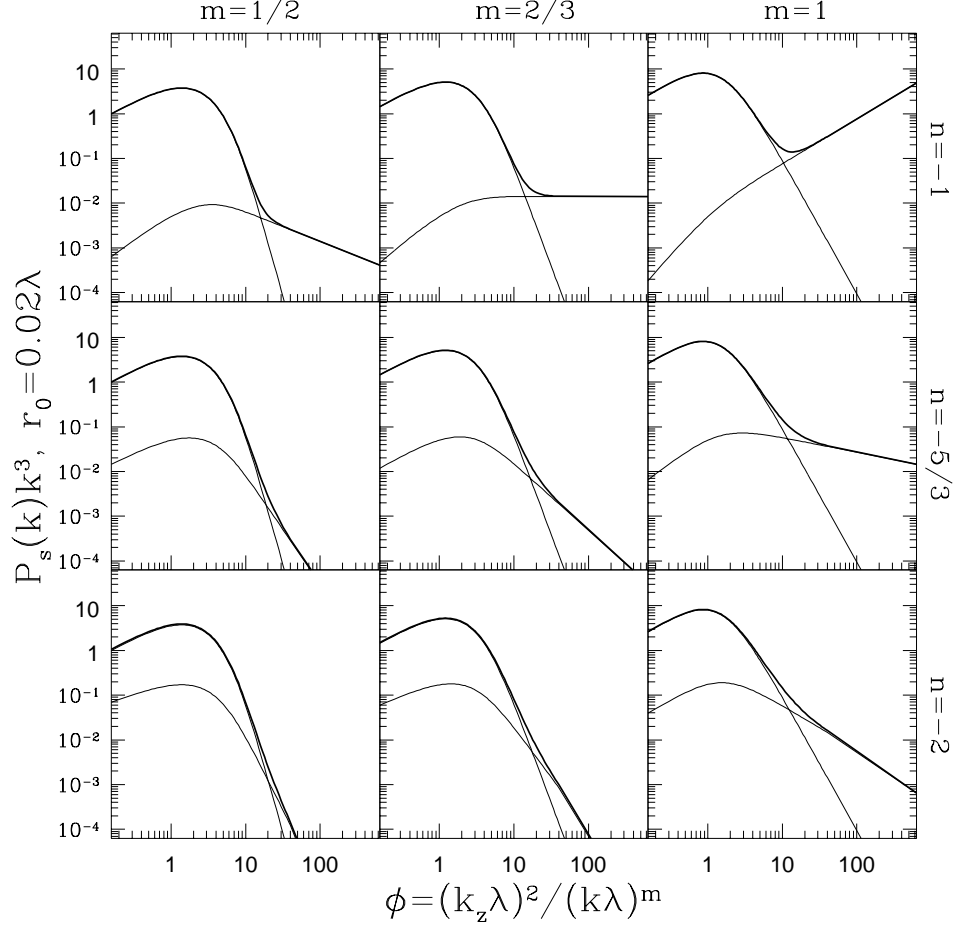


FIG. B7.— The same as in Fig. B6 but for $r_0 = 0.02\lambda$.

	$(r/\lambda) \rightarrow 0$	$(r/\lambda) \rightarrow \infty$
$(\lambda/r_0)^\gamma \xi_\rho(R, 0) :$	$C_{\gamma m} \cdot (R/\lambda)^{-\gamma+(1-m/2)}$	$(R/\lambda)^{-\gamma}$
$(\lambda/r_0)^\gamma \xi_\rho(0, z_s) :$	$c_{\gamma m} \cdot (z_s/\lambda)^{-\gamma-\frac{(2-m)}{m}(\gamma-1)}$	$(z_s/\lambda)^{-\gamma}$
$\xi_v(R, 0) :$	$m/(2-m)$	$(m^2/4) \cdot (R/\lambda)^{m-2}$
$\xi_v(0, z_s) :$	$m/(2-m)$	$\frac{m(m-1)}{2} \cdot (z_s/\lambda)^{m-2}$

TABLE C3

ASYMPTOTICAL BEHAVIOR OF THE CORRELATION FUNCTION IN VELOCITY SPACE. NUMERICAL CONSTANTS $c_{\gamma m}$ AND $C_{\gamma m}$ ARE GIVEN IN APPENDIX A.

The term ξ_v has a finite value at a zero separation and is not important at small distances. Correlation at the very long distances is, however, dominated by velocity term if $\gamma > 2 - m$. The above results are illustrated in Fig. C8.

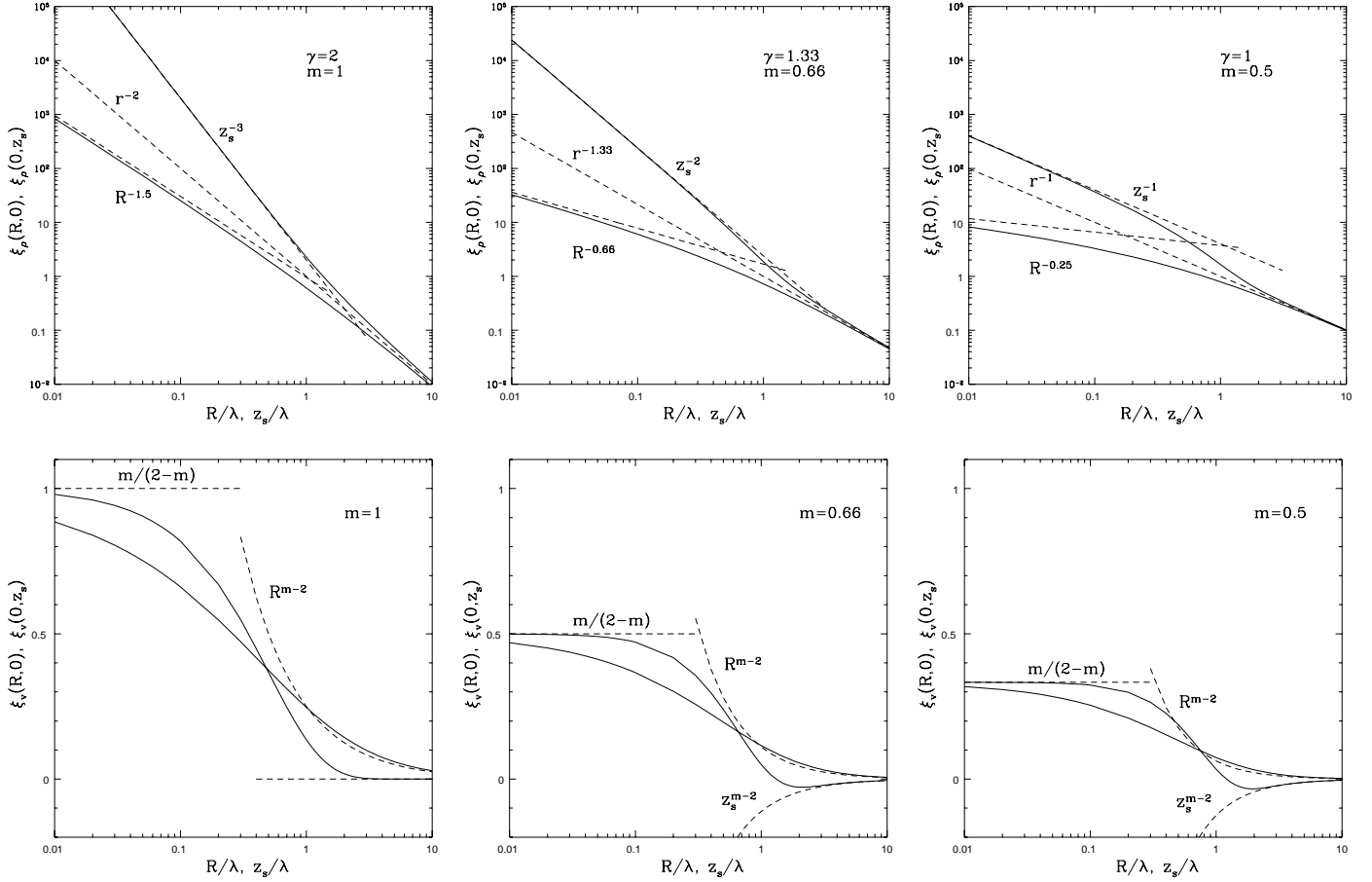


FIG. C8.— Correlation function in velocity space for various choice of γ and m . Upper set of panels shown the density term ξ_ρ the line of sight, $\xi_\rho(R, 0)$, and in a transverse *thin* slice, $\xi_\rho(0, z_s)$. Asymptotics also include underlying $r^{-\gamma}$ slope for density correlation function before velocity mapping.

In view of large values of λ the regime $r/\lambda \rightarrow 0$ is the most important.

CORRELATIONS BETWEEN DENSITY AND VELOCITY

Our assumption in the body of the paper was that the density and velocity are uncorrelated. Therefore it is interesting to study whether possible velocity-density correlations alter our result. To do this we have to assume a statistical model for the density field.

In what follows we shall consider the Lognormal density distribution. Particularly, we assume that the density can be expressed as the exponent of the Gaussian field $z(\mathbf{x})$,

$$\rho(\mathbf{x}) = \rho_0 e^{z(\mathbf{x})}. \quad (\text{D1})$$

The advantage of this model for density is that it can describe nonlinear density fluctuations $|\delta| > 1$ while remaining simple³⁴.

We parametrize the Gaussian distribution for $z(\mathbf{x})$ in the following way

$$P(z) = \frac{1}{(2\pi)^{1/2} A^{1/2}} \exp\left[-\frac{z^2}{2A}\right] \quad (\text{D2})$$

³⁴The Gaussian model of the density field cannot describe large fluctuations and therefore we do not consider it.

Then the average and the second moment of the density distribution, which can be directly measured, are related to the parameters ρ_0 and A as

$$\begin{aligned}\bar{\rho} &\equiv \langle \rho \rangle = \rho_0 e^{A/2} \\ \sigma_\rho^2 &\equiv \langle \rho^2 \rangle = \rho_0^2 e^{2A}\end{aligned}\quad (\text{D3})$$

In the absence of density inhomogeneities $A \rightarrow 0$, $\bar{\rho} \rightarrow \rho_0$.

Power spectrum in velocity space is a Fourier transform of the kernel (see eq. (7))

$$\langle e^{ifk_z[u_z(1)-u_z(2)]} \rho(1)\rho(2) \rangle \quad (\text{D4})$$

where u_z is z-component of velocity, ρ and 1, 2 refer to two points in space, k_z is a wavevector component in the velocity space.

To calculate the statistical average in eq. (D4) we use the variables

$$y \equiv f/\lambda [u_z(1) - u_z(2)] \quad (\text{D5})$$

$$z_+ \equiv z(1) + z(2) \quad (\text{D6})$$

which are Gaussian random quantities obeying bivariant joint Gaussian distribution. It is well known that a general Gaussian distribution of N correlated variables (with a zero mean values) described by a vector $\mathbf{X} = (x_1, x_2, \dots, x_N)$ is given by the probability function

$$\begin{aligned}P(x_1, x_2, \dots, x_N) &= \frac{1}{(2\pi)^{N/2} \|\mathbf{C}\|^{1/2}} \exp \left[-\frac{1}{2} \mathbf{X} \mathbf{C}^{-1} \mathbf{X} \right] \\ \mathbf{C} &\equiv \begin{pmatrix} \langle x_1^2 \rangle & \langle x_1 x_2 \rangle & \dots & \langle x_1 x_N \rangle \\ \langle x_1 x_2 \rangle & \langle x_2^2 \rangle & \dots & \langle x_2 x_N \rangle \\ \dots & \dots & \dots & \dots \\ \langle x_1 x_N \rangle & \langle x_2 x_N \rangle & \dots & \langle x_N^2 \rangle \end{pmatrix}\end{aligned}\quad (\text{D7})$$

We shall characterize the correlation properties of a pair (y, z_+) by three functions

$$\begin{aligned}\langle y^2 \rangle &= D_z(\mathbf{r}) \\ \langle z_+^2 \rangle &= B(\mathbf{r}) \\ \langle y z_+ \rangle &= \langle u_z(1) z(2) \rangle - \langle u_z(2) z(1) \rangle \equiv F(\mathbf{r})\end{aligned}\quad (\text{D8})$$

where $F(\mathbf{r})$ is a cross correlation function³⁵ of velocity and density, $D_z(\mathbf{r})$ is the z-projection of velocity structure function given by eq (17) and $B(\mathbf{r})$ can be expressed through the density correlation function $\xi(\mathbf{r})$. Substituting those functions in eq. (D7) we get the joint distribution function

$$P(y, z_+) = \frac{1}{2\pi(D_z B - F^2)^{1/2}} \exp \left\{ -\frac{B y^2 - 2F y z_+ + D_z z_+^2}{2(D_z B - F^2)} \right\}, \quad (\text{D9})$$

using which one can easily compute that

$$\xi(\mathbf{r}) \equiv \langle \rho(1)\rho(2) \rangle / \rho_0^2 = \langle e^{z_+} \rangle = e^{B(\mathbf{r})/2}, \quad (\text{D10})$$

and, thus, $B(0) = 4A = 2 \ln \sigma_\rho^2 / \rho_0^2$.

³⁵In the equation for $F(\mathbf{r})$ we have used the fact that a random vector quantity (velocity in our case) always has a zero correlation with any scalar quantity (as density) at the same location in space, i.e., $\langle u_z(1)\rho(1) \rangle = \langle u_z(2)\rho(2) \rangle = 0$. Indeed, the correlation functions of density-velocity in one point can be obtained by correlating velocity and density in two different points 1 and 2 and then bringing the points together. It is obvious that if points 1 and 2 are along z-axis and very close together, $\langle u_z(1)\rho(2) \rangle \approx -\langle u_z(2)\rho(1) \rangle$. This proves that the correlations are zero when the points coincide.

Averaging kernel (D4) with the distribution function given by eq. (D9) yields

$$P_s(\mathbf{K}, k_z) = \int d^3\mathbf{r} e^{i\mathbf{k}\cdot\mathbf{r}} \exp\left[-\frac{(k_z\lambda)^2 D_z(\mathbf{r})}{2}\right] \exp[ik_z\lambda F(\mathbf{r})] \xi(\mathbf{r}) \quad , \quad (\text{D11})$$

which generalizes eq.(16) for a non-zero correlation of velocity and density.

Let us now project P_3 to P_2 in a *thin* slice and for high $|\mathbf{K}|$. Using eq. (26) and P_s given by eq. (D11) we obtain

$$P_2(\mathbf{K}) \approx \frac{1}{(2\pi)^{1/2}\lambda} \int d\mathbf{r} e^{i\mathbf{K}\mathbf{r}} \frac{\xi(\mathbf{r})}{D_z^{1/2}(\mathbf{r})} \exp\left[-\frac{F^2(\mathbf{r})}{2D_z(\mathbf{r})}\right] \exp\left[-\frac{z^2}{2\lambda^2 \tilde{D}_z(\mathbf{r}/\lambda)}\right] \quad (\text{D12})$$

This expression is an analog of eq. (29) in section 3 for $F \neq 0$. For high $|\mathbf{K}|$ the last exponent may be shown to be ≈ 1 and then the equation become analogous to eq. (40).

An upper limit for F cross-correlation function follows from general Cauchy-Swartz inequality (see Mathews & Walker 1970), $\langle yz_+ \rangle^2 \leq \langle y^2 \rangle \langle z_+^2 \rangle$,

$$F^2(\mathbf{r}) \leq D_z(\mathbf{r})B(\mathbf{r}) = 2D_z(\mathbf{r}) \ln \xi(\mathbf{r}). \quad (\text{D13})$$

and this limiting case is achieved when density (logarithm) and velocity are perfectly correlated and are not independent statistical quantities. If we adopt this limit, $\xi(\mathbf{r})$ cancels out and the velocity fluctuations in the thin slice limit are determined by the spectrum of random velocity only:

$$P_2(\mathbf{K})|_t \approx \frac{1}{(2\pi)^{1/2}\lambda} \int d\mathbf{r} e^{i\mathbf{K}\mathbf{r}} D_z^{-1/2} \quad (\text{D14})$$

It is easy to see that equation eq. (D14) coincides with the expression for P_{2v} and therefore in the case of long-wave dominated density field we reproduce the thin-slice asymptotics found on the assumption of no correlation of velocity and density. Indeed, our analysis in section 4 showed that in this regime the P_{2v} part of the spectrum dominates the signal. Formally, we do not reproduce the result for the short-wave dominated density regime, where $P_{2\rho}$ part of P_2 is important. However, we assumed the absolute maximum (unrealistic!) of the velocity-density correlations. Therefore, for more realistic cases we do expect density to reveal itself within the thin slices in the regime of short-wave density fluctuations.

Eq. (D11) also indicate that the criterion for the velocity slice to be thick may be altered if the velocity-density correlations are present. Apart from the criterion (35) one need to require that $\mathcal{L}/\lambda > (1/\lambda|\mathbf{K}|)F$. For realistically small F this condition is fulfilled when (35) is fulfilled. In the case of upper limit of correlation given by eq. (D13) the thickness of the slice should be increased by a factor of the order of a few. Asymptotics in the regime of thick slicing given by Table 1 stay the same when velocity-density are correlated.

All in all, thick slice regime does not depend on velocity and density being correlated. This regime can provide us with the information whether density is long or short wave correlated. The density dominates for “very thick” slices (see criterion (50)) and for them it is possible to determine the density spectrum irrespectively of velocity-density correlations. The regime of thin slices depends on the velocity random field if the density field is long-wave correlated and the spectra of both velocity and density field if the density is short-wave correlated (see Table 1). In the case of a thin slice we recover the velocity power spectrum for the long-wave dominated regime. The only limiting case when velocity-density correlations can matter is the thin slice for the short-wave dominated density field. In the extreme case of a perfect velocity-density correlation the emissivity depends only on the velocity spectrum, while the emissivity does depend on density if the correlations are absent. This means that if the analysis of the thick sliced data reveals short-wave correlated density, an additional care for the analysis of the data in the thin slice regime might be needed.

Our analysis of velocity-density correlations was performed for the case of the HI turbulence study in Galactic disc. However, it is also applicable to the studies of turbulence in individual clouds (see Appendix E).

APPLICATION TO INDIVIDUAL CLOUDS

In the main body of the paper we were concerned with the studies of HI in the Galactic disc when the Galactic rotation curve served as a distance indicator. If studies of individual clouds are concerned (e.g. high latitude clouds) no analog of the distance-velocity relation exists. Similar problems arise when we deal with external galaxies.

Here we derive the expression for 2D spectrum of HI emission applicable to studies of turbulence within individual clouds. To do this we modify our formalism presented in the main text to account for the finite size of the emitting region. We will generalize map (2):

$$\begin{aligned} \mathbf{X}_s &= \mathbf{X} \\ z_s &= A \left[f^{-1}z - \mathbf{u}(\mathbf{x}) \cdot \hat{\mathbf{z}} \right] \quad , \end{aligned} \quad (\text{E1})$$

where the parameter A is just a conversion factor which specifies the units of z_s coordinate. Our previous map (2) corresponds to the choice $A = f$. In the present form the map is applicable to a zero shear, which corresponds to $f^{-1} \rightarrow 0$.

Our further treatment of the problem repeats the steps discussed in the main text but we take into account the finite extend of the cloud. Since in the image plane we consider only short scales relative to our object size, we can simplify our task by accounting for only for a finite thickness S of the cloud along the line-of-sight. In place of eq.(4) the Fourier component of density in velocity space is now

$$\rho_s(\mathbf{k}) = \int_0^S dz e^{iAf^{-1}k_z z} \int d^2\mathbf{X} e^{i\mathbf{K} \cdot \mathbf{X}} \rho(\mathbf{x}) e^{-iAk_z u_z(\mathbf{x})} \quad , \quad (\text{E2})$$

where line-of-sight and image plane transforms are now treated separately and we use convention $\mathbf{k} = (\mathbf{K}, k_z)$.

To calculate the statistical average $\langle \rho_s(\mathbf{k}) \rho_s^*(\mathbf{k}') \rangle$ for Fourier components of the density in velocity space we assume statistical homogeneity for the quantities in real space, which entails that

$$\Xi_2(k_z, k'_z, \mathbf{r}) = \langle \rho(\mathbf{x}) \rho(\mathbf{x}') e^{iA[k_z \mathbf{u}(\mathbf{x}) \cdot \hat{\mathbf{z}} - k'_z \mathbf{u}(\mathbf{x}') \cdot \hat{\mathbf{z}}]} \rangle \quad (\text{E3})$$

depends only on the difference $\mathbf{r} \equiv \mathbf{x} - \mathbf{x}'$. Choosing new variables \mathbf{r} and $\mathbf{x}^+ = (\mathbf{x} + \mathbf{x}')/2$ we obtain ³⁶

$$\langle \rho_s(\mathbf{k}) \rho_s^*(\mathbf{k}') \rangle = 2\delta(\mathbf{K} - \mathbf{K}') \int_0^S dr_z \int_{r_z/2}^{S-r_z/2} dz^+ \int d^2\mathbf{R} \Xi_2(k_z, k'_z, \mathbf{R}, r_z) e^{i\mathbf{K}\mathbf{R}} e^{iAf^{-1}[k_z^- z^+ - k_z^+ r_z]} \quad (\text{E5})$$

Here $k_z^+ = (k_z + k'_z)/2$ and $k_z^- = k_z - k'_z$.

Assuming that density and velocity fields in galactic coordinates are uncorrelated (cf. Appendix D) and described by a correlation $\xi(r)$ and structure (see eq. (11)) functions we get

$$\Xi_2(k_z, k'_z, \mathbf{r}) = \xi(r) e^{-\frac{1}{2}A^2[(k_z - k'_z)^2 D_z(\infty)/2 + k_z k'_z D_z(\mathbf{r})]} \quad (\text{E6})$$

Important feature of eq. (E6) compared to the kernel in the main text is the explicit presence of the velocity dispersion $\langle u_z^2 \rangle = D_z(\infty)/2$ in the exponent, since we have to treat k_z and k'_z as separate. This means that one cannot use pure power-law structure functions to describe velocity turbulence,

³⁶Depending on convenience, we choose one of the following transformations of the double integral along a pair of lines-of-sight through the slice of finite thickness, $z_+ = (z + z')/2$, $z^- = z - z'$:

$$\begin{aligned} \int_0^S dz \int_0^S dz' F(z, z') &= \int_0^S dz^- \int_{z^-/2}^{S-z^-/2} dz^+ [F(z^+, z^-) + F(z^+, -z^-)] \\ &= \int_0^{S/2} dz^+ \int_{-2z^+}^{2z^+} dz^- [F(z^+, z^-) + F(S - z^+, z^-)] \end{aligned} \quad (\text{E4})$$

but the turbulence must have a maximum scale. This is perfectly in line with the introduction of finite cloud size along the line-of-sight. In the absence of additional physics the size S also serves as cutoff scale for the structure function $D(r) \sim D(\infty)r^m/(r^m + S^m)$, but we notice that if this law is adopted for $D_{LL}(r)$, z-component of the structure function in the case of solenoidal turbulence is

$$D_z(\mathbf{r}) = D(\infty) \frac{r^m}{r^m + S^m} \left(1 + \frac{m/2}{1 + (r/S)^m} (1 - \cos^2 \theta) \right), \quad \cos \theta = \mathbf{r} \cdot \hat{\mathbf{z}}/r \quad (\text{E7})$$

$$D_z(\infty) = D(\infty) = CS^m \quad (\text{E8})$$

For clouds introduce in Appendix F 3D spectrum in velocity space, but here use eq. (E5) directly to obtain 2D spectrum of intensity in velocity slice from eq. (20). Expressing left-hand-side intensity correlation function as the Fourier integral of $P_2(\mathbf{K})$ (see eq. (22)) and right-hand-side 3D density correlation in velocity space as double Fourier integral of the $\langle \rho_s(\mathbf{k})\rho_s(\mathbf{k}') \rangle$ given by eq. (E5) we can carry out integration over k_z and k'_z to obtain

$$P_2(\mathbf{K}) \propto \int d^2\mathbf{R} e^{i\mathbf{K}\mathbf{R}} \int_0^{\delta V} dz_s^- \int_{z_s^-/2}^{\delta V - z_s^-/2} dz_s^+ \times \quad (\text{E9})$$

$$\int_0^S \frac{1}{[B_1(\mathbf{r})D_z(\mathbf{r})]^{1/2}} e^{-(f^{-1}r_z - z_s^-)^2/B(\mathbf{r})} \int_{r_z/2}^{S-r_z/2} dz^+ e^{-(f^{-1}z^+ - z_s^+)^2/2D_z(\mathbf{r})} \xi(\mathbf{R}, r_z)$$

where $B_1(\mathbf{r}) = D(\infty)[1 - D_z(\mathbf{r})/2D(\infty)]$ only weakly depends on r and $\sim D(\infty)$. Since our z_s coordinates are in velocity units, integration over them is done directly through velocity slice of δV width. As one expects, parameter A drops out of equations. Although eq. (E9) can be further evaluated, resulting error functions are not very illuminating. We shall analyze the limit $f^{-1} \rightarrow 0$ instead, which describes the case when coherent motions through the cloud can be neglected. It is useful to change the order of integration over z_s^+ and z_s^- according to (E4). Then

$$P_2(\mathbf{K}) \propto \int d^2\mathbf{R} e^{i\mathbf{K}\mathbf{R}} \int_0^S dr_z (S - r_z) \int_0^{\delta V} dz_s^+ \frac{e^{-z_s^{+2}/B_1(\mathbf{r})} + e^{-(\delta V - z_s^+)^2/B_1(\mathbf{r})}}{B_1^{1/2}(\mathbf{r})} \text{erf} \left[\frac{z_s^+}{(D_z/2)^{1/2}} \right] \xi(\mathbf{R}, r_z) \quad (\text{E10})$$

The structure of this expression looks somewhat different from eq. (23) mainly because here we have first performed integration over k_z , rather than z_s . This form is convenient to discuss variation of the result with the slice thickness. We can now distinguish three regimes. If the velocity slice is *thick*, namely larger than velocity dispersion on the scale of the cloud $\delta V \gg B_1^{1/2} \sim D^{1/2}(\infty)$, then an integration over the whole line (i.e. up to infinity) is appropriate

$$P_2(\mathbf{K}) \propto \int d^2\mathbf{R} e^{i\mathbf{K}\mathbf{R}} \int_0^S dr_z (S - r_z) \tan^{-1} \left[(B_1/2D_z)^{1/2} \right] \xi(\mathbf{R}, r_z) \quad (\text{E11})$$

The velocity effects disappear in this regime, with only minor residuals through the almost constant function \tan^{-1} .

When the slice is not very thick, $\delta V \ll D^{1/2}(\infty)$, exponential terms in eq. (E10) are close to unity and one returns to the situation discussed in the paper. Namely, the slice is *thin* when $\delta V < D_z^{1/2}(|\mathbf{K}|^{-1})$. Then the error function in eq. (E10) can be expanded in series and in the leading order

$$P_2(\mathbf{K})|_t \propto \int d^2\mathbf{R} e^{i\mathbf{K}\mathbf{R}} \int_0^S dr_z (S - r_z) B_1^{-1/2}(\mathbf{r}) \frac{\xi(\mathbf{R}, r_z)}{D_z^{1/2}(\mathbf{r})^{1/2}} \quad (\text{E12})$$

This recovers the eq. (40) with modification for the finite size of the cloud³⁷. As $B_1(\mathbf{r})$ varies slowly with \mathbf{r} it can be considered as a constant $\approx D(\infty) \approx CS^m$. Indeed, it is easy notice (see eq. (E8)) that

³⁷The presence of r_z in eq. (E12) results in a subdominant term that decreases faster than the main term for large $|\mathbf{K}|$.

$D_z(\mathbf{r})/CS^m = \{(\mathbf{r}/S)$ which plays the role of $D_z(\mathbf{r}/\lambda)$ in eq. (40). Thus the size of the cloud S plays the role of the correlation scale λ . Also, the physically transparent condition $\delta V < D_z^{1/2}(|\mathbf{K}|^{-1})$ exactly corresponds to the transition point between thin and thick slice regimes derived earlier in (36). The fact that in a completely different regime we obtained the same condition for the separation between thin and thick slices shows that this condition is universal and the cancellation of f in eq. (36) was not accidental. This finding allows us to apply our theory to both individual clouds and to external galaxies without caring too much about a regular shear. The thick and thin slice asymptotics are given by Table 1 with S being used instead of λ .

The effects of the emitting region being finite is seen in the thick slice regime. This regime corresponds to an intermediate value of δV , $D_z^{1/2}(|\mathbf{K}|^{-1}) < \delta V < D^{1/2}(\infty)$. Obviously enough, the integration over the full velocity dispersion provides the statistics that depends only on the density field. Inversion of this statistics provides the 3D density power spectrum as it is shown in L95.

The opportunity of determining density spectrum before dealing with the velocity is very welcome. In other words, individual HI clouds present an excellent example for studying the interstellar statistics. Our results here are directly applicable to optically thin species in molecular clouds.

1D SPECTRUM ALONG LINE OF SIGHT

Calculation of the one dimensional power spectrum along a line-of-sight $P_1(k_z)$ in velocity space is very straightforward under assumptions adopted in the paper. Indeed

$$P_1(k_z) = \int d\mathbf{K} P_s(\mathbf{K}, k_z) \quad (\text{F1})$$

or, using eq. (16)

$$P_1(k_z) = e^{-f^2 k_z^2 v_T^2} \int dz e^{ik_z z} \xi(z) \exp \left[-\frac{(k_z \lambda)^2 \tilde{D}_z(z/\lambda)}{2} \right], \quad (\text{F2})$$

Asymptotics for the density $P_{1\rho}$ part (described by a correlation function $\xi(r) \propto r^{-\gamma}$) and velocity term P_{1v} (which corresponds to $\xi(r) = \text{const}$) are given in the table:

$k_z \lambda \ll 1$; $k_z \lambda \gg 1$	
$\lambda^{-1}(\lambda/r_0)^{3+n} P_{1\rho}(k_z) :$	$(k_z \lambda)^{n+2}; \quad (k_z \lambda)^{2(n+2)/m}$
$\lambda^{-1} P_{1v}(k_z) :$	$(k_z \lambda)^{1-m}; \quad (k_z \lambda)^{-2/m}$

TABLE F4

ASYMPTOTICS OF THE 1D SPECTRUM ALONG THE LINE OF SIGHT AT SCALES LARGER THAN GAS SOUND SPEED, $k_z < 1/(fv_T)$.

This results are valid for $\gamma < 1$, so $n < -2$. At velocity scales below gas sound speed $k_z > 1/(fv_T)$ the line-of-sight power is suppressed. Note that the expression for $P_{1\rho}$ term in the longwave regime would correspond to the density spectrum along the line-of-sight in the absence of velocity mapping. The asymptotics are illustrated by the full solution, available for $m = 1$ case.

$$P_1(k_z) \propto e^{-(k_z \lambda)^2 (fv_T/\lambda)^2} \cos \left[(n+2) \tan^{-1}(1/k_z \lambda) \right] \left[(k_z \lambda)^2 (1 + (k_z \lambda)^2) \right]^{(n+2)/2} \quad (\text{F3})$$

To get P_{1v} term one should substitute -3 instead of n . This spectrum allows to distinguish the short and long-wave density regime easily.

For all practical purposes in the case of the Galaxy λ is sufficiently large that we shall be in $k_z\lambda \gg 1$ regime. In this regime the scale when the contribution from P_{1v} and $P_{1\rho}$ terms are equal is

$$(k_z\lambda)^{2/m} = \lambda/r_0 \quad (\text{F4})$$

and does not depend on n . However, which scales are dominated by the P_{1v} term and which by the $P_{1\rho}$ term does depend on whether $n < -3$ or $n > -3$. If the underlying spectrum is steep, $n < -3$, the short scales $k_z\lambda > (\lambda/r_0)^{m/2}$ are dominated by velocity term while the intermediate scales $1 < k_z\lambda < (\lambda/r_0)^{m/2}$ are determined by the density. The situation is reversed for shallow $n > -3$ spectra. As a consequence, the spectrum on small scales always has shallower slope than on the intermediate ones.

We can incorporate the effect of finite thickness of the cloud as follows. Let us model the density field inside cloud as $\rho_{cl}(\mathbf{x}) = \rho(\mathbf{x}) \cdot F(\mathbf{x}, \mathbf{S})$ where $\rho(\mathbf{x})$ is statistically homogeneous random field, while $F(\mathbf{x})$ describes the shape of the cloud. We assume the cloud is centered at the origin and has characteristic size S . This size, in principle, can be different in different directions, thus the vector notation. Similarly to eq. (5) we obtain for the power spectrum in velocity space

$$\langle \rho_s(\mathbf{k}) \rho_s^*(\mathbf{k}) \rangle = e^{-f^2 k_z^2 v_T^2} \int d^3 \mathbf{r} e^{i\mathbf{k} \cdot \mathbf{r}} \Xi(\mathbf{k}, \mathbf{r}) \int d^3 \mathbf{x}_+ F(\mathbf{x}_+ + \mathbf{r}/2, \mathbf{S}) F(\mathbf{x}_+ - \mathbf{r}/2, \mathbf{S}) . \quad (\text{F5})$$

where $\mathbf{x}_+ = (\mathbf{x} + \mathbf{x}')/2$ (compare to eq. (5)). Note, that different Fourier components are not formally orthogonal when we deal with finite clouds. We did not write down the off-diagonal elements, but the diagonal ones, in contrast to eq. (7) contain not a delta-finction, but a convolution of shape functions F . This convolution is the easiest to evaluate in Fourier space

$$F^2(\mathbf{r}, \mathbf{S}) \equiv \int d^3 \mathbf{x}_+ F(\mathbf{x}_+ + \mathbf{r}/2, \mathbf{S}) F(\mathbf{x}_+ - \mathbf{r}/2, \mathbf{S}) \propto \int d^3 \mathbf{k} F^2(\mathbf{kS}) e^{i\mathbf{k} \cdot \mathbf{r}} \quad (\text{F6})$$

1D power spectrum with finite cloud size taken into account is giving by a modified version of eq. (F2)

$$P_1(k_z) = e^{-f^2 k_z^2 v_T^2} \int dz e^{ik_z z} \xi(z) \exp \left[-\frac{(k_z \lambda)^2 \tilde{D}_z(z/\lambda)}{2} \right] F^2(z, S_z) \quad , \quad (\text{F7})$$

The modification is insignificant for high $k_z > S_z^{-1}$ since at small scales shape function is constant and we can use asymptotics in Table (F4). To prove this consider a spherical cloud of constant density, $F(r/S) = \text{const}$, $r \leq S/2$; $F(r/S) = 0$, $r > S/2$. Then

$$F^2(z/S) \propto 1 - \frac{3}{2}|z/S| + \frac{1}{2}|z/S|^3, \quad |z/S| \leq 1 \quad (\text{F8})$$

This is somewhat different from a model with a finite thickness S of the cloud along the line-of-sight, infinite dimensions in the image plane. In this case

$$F^2(z/S) \propto 1 - |z/S|, \quad |z/S| \leq 1 \quad (\text{F9})$$

Note, that in both expressions above for $z \ll S$ only unity term matters and for small scale turbulence eq. (F5) presents the 3D spectrum in velocity space.

The 1D statistics is complimentary to the 2D statistics that we dwelt upon in the main text. Applying 1D spectral analysis to data cubes it is possible to determine whether the spectrum is long-wave or short-wave dominated.

REFERENCES

- Arnold, V.I., Gussein-Zade, S.M., Varchenko, A.N., 1985, *Singularities of Differentiable Maps*: Birkhausen Boston, Cambridge, 432.
- Armstrong, J.M., Rickett, B.J., & Spangler, S.R. 1995, *ApJ*, 443, 209
- Benson, P. J., & Myers, P. C. 1989, *ApJS*, 71, 89
- Blitz, L. & Spergel, D.N. 1991, *ApJ*, 370, 205
- Boss, A.P. 1987, *Phases of the Interstellar Medium*, in *Interstellar Processes*, eds Hollenbach D.J. and Thronson H.A., Reidel, Dordrecht, p. 321
- Boulanger F., Abergel, A., Bernard J.-P., Burton, W.B., Desert, F.-X., Hartman, D., Lagache, G., Puget J.-L. 1996, *A&A*, 312, 256
- Braun, R. 1997, *ApJ*, 484, 637
- Braun, R. 1999, *Properties of Atomic Gas in Spiral Galaxies*, in *Interstellar Turbulence*, eds. Jose Franco & Alberto Carraminana, CUP, p. 12
- Burton, W.B., 1992, *Distribution and Observational Properties of the ISM*, in *Galactic Interstellar Medium*, Pfenninger D., Bartholdi P., Springer-Verlag, p. 1
- Crovisier, J. & Dickey, M. 1983, *A&A*, 122, 282
- Dickey, J.M., 1995, in "The Physics of the Interstellar Medium and Intergalactic Medium", eds Ferrara A., McKee C.F., Heiles C., Schapiro P.R., ASP Conf. Ser. V80.
- Dickman, R.L., 1985, *Turbulence in Molecular Clouds*, in *Protostars and Planets II*, eds Black D.C. and Mathews M.S., Tucson: University of Arizona, 150
- Dickman, R.L. & Kleiner, S.C. 1985, *ApJ*, 295, 479
- Draine B.T. & Lazarian, A. 1999, in "Sloan Summit on Microwave Foregrounds", ed. A. de Oliveira-Costa and M. Tegmark
- Draine B.T. & Lazarian, A. 1998, *ApJ*, 494, L19
- Elmegreen, B.G. 1994, *Infrared Cirrus and Interstellar Diffuse Clouds*, ed. Roc Cutri and Bill Latter, A.S.P., V58, 380
- Falgarone, E. et al. 1998, *A&A*, 331, 669
- Gautier, T.N., Boulanger, F., Pérault, M. & Puget, J.-L. 1992, *AJ*, 103, 1313
- Goldreich, P. & Sridhar, S. 1995, *ApJ*, 438, 763
- Goodman, A.A. 1999, <http://cfa-www.harvard.edu/~agoodman/scf/SCF/scfmain.html>
- Goodman, J., & Narayan, R. 1985, *MNRAS*, 214, 519
- Green, D.A. 1993 *MNRAS*, 262, 328
- Green, D.A. 1994 *Ap&SS*, 216, 61
- Hamilton, A.J.S. 1998, in *The Evolving Universe*, ed. D. Hamilton (Dordrecht:Kluwer), 185
- Heiles, C. in *Polarimetry of the Interstellar Medium*, eds Roberge W.G. and Whittet, D.C.B., APS Conf. Series 97,457
- Heithausen, A., & Thaddeus, P. 1990, *ApJ*, 353, L49
- Henriksen, R.N. 1994, *Ap&SS*, 221, 25
- Heyer, M. et al. 1997, *FCRAO newsletter*, vol. 8, p.6
- Higgs, L.A. (1999), *The Canadian Galactic Plane Survey: Atomic Hydrogen Observations*, in *New Perspectives on the Interstellar Medium*, ASP 168, p. 15
- von Horner, S. 1951, *Zs.F. Ap.*, 30, 17
- Houllahan, P., Scalo J., 1990, *ApJ*, 72, 133.
- Iroshnikov, P.S. 1963, *AZh*, 40, 742
- Kaiser, N., 1987 *MNRAS*, 227, 1.
- Kaplan, S.A. & Pickelner, S.B. 1970, *The Interstellar Medium*, Harvard University Press
- Kerr, F.J. & Lynden-Bell, D. 1986, *MNRAS*, 221, 1023
- Kolmogorov, A. 1941, *Compt. Rend. Acad. Sci. USSR*, 30, 301
- Kraichnan, R.H. 1965, *Phys. Fluids*, 8, 1385
- Kramer, C., Stutzki, J., Rohrig, R., & Corneliussen, U. 1998, *A&A*, 329, 249
- Langer, W.D., Wilson, R.W., & Anderson, C.H. 1993, *ApJ*, 408, L45
- Larson, R. 1992, *MNRAS*, 26, 641
- Lazarian, A. 1992, *Astron. and Astrophys. Transactions*, 3, 33
- Lazarian, A. 1993, *Applied Scientific Research*, 51, 191
- Lazarian, A. 1994a, *Plasma Phys. and Contr. Fusion*, 36, 1013
- Lazarian, A. 1994b, PhD Thesis, University of Cambridge
- Lazarian, A. 1995, *A&A*, 293, 507
- Lazarian, A. 1999a, *Turbulence in Atomic Hydrogen*, in *Interstellar Turbulence*, eds. Jose Franco & Alberto Carraminana, CUP, p.95, astro-ph/9804024
- Lazarian, A. 1999b, *Statistics of Turbulence from Spectral-line Data Cubes*, in *Plasma turbulence and energetic particles*, ed. M. Ostrowski and R. Schlickeiser, Cracow, 000, astro-ph/0001001
- Lazarian, A. & Pogosyan, D. 1997, *ApJ*, 491, 200
- Lazarian, A., & Vishniac, E. 1999, *ApJ*, 517, 700
- McKee, C.F. & Ostriker, J.P. 1977, *ApJ*, 218, 148
- Miesch, M.S., & Bally, J. 1994, *ApJ*, 429, 645
- Monin, A.S., & Yaglom, A.M. 1975, *Statistical Fluid Mechanics: Mechanics of Turbulence*, vol. 2, The MIT Press
- Myers, P.C., & Lazarian, A. *ApJ*, 507, L157
- Munch, G. 1958, *Rev. Mod. Phys.*, 30, 1035
- Narayan, R. 1992, *Phil. Trans. Royal Soc.*, 341, 151
- Narayan, R., & Goodman, J. 1989, *MNRAS*, 238, 963
- O'Dell, C.R. 1986, *ApJ*, 304, 767
- O'Dell, C.R., & Castaneda, H.O. 1987, *ApJ*, 317, 686
- Prunet, S. & Lazarian, A. 1999, in "Sloan Summit on Microwave Foregrounds", ed. A. de Oliveira-Costa and M. Tegmark
- Rosolowsky, E.W., Goodman, A.A., Wilner, D.J., & Williams, J.P. 1999, *ApJ*, in press
- Scalo, J.M. 1985, *Fragmentation and Hierarchical Structure in the Interstellar Medium*, in *Protostars and Planets II*, eds Black D.C. and Mathews M.S., Tucson: University of Arizona, 201
- Scalo, J.M. (1987), *Theoretical approaches to interstellar turbulence*, in *Interstellar Processes*, eds. D.F. Hollenbach & H.A. Thronson, Reidel, Dordrecht, 349
- Scalo, J.M., Lazarian, A. 1996, *ApJ*, 469, 189
- Scoccimarro, R. 1997, *ApJ*, 487, 1
- Scoccimarro, R., Couchman, H.M.P., & Frieman, J. 1999, *ApJ*, 517, 531
- Sethi, S.K., Prunet, S., Bouchet, F.R., 1998, astro-ph/9803158.
- Shull, J.M. 1987, *Phases of the Interstellar Medium*, in *Interstellar Processes*, eds Hollenbach D.J. and Thronson H.A., Reidel, Dordrecht, 225
- Spangler, S.R., & Gwinn, C.R. 1990, *ApJ*, 353, L29
- Spicker, J., & Feitzinger, J. V. 1988b, *A&A*, 191, 186
- Spitzer L., Jr 1978, *Physical Processes in the Interstellar Medium*, Wiley-Interscience, New York
- Spoelstra, T.A.Th. & Brouw, W.A. 1976, *A&AS*, 26, No.1
- Stanimirovic, S., Staveley-Smith, L., Dickey, J.M., Sault, R.J., & Snowden, S.L. 1999, *MNRAS*, 302, 417
- Stanimirovic, S., Staveley-Smith, L., van der Hulst, J.M., Bontekoe, Tj.R., Kester, D.J.M., Jones, P.A. 2000, *MNRAS*, submitted
- Stutzki, J., Bensch, F., Heithausen, A., Ossenkopf, V., & Zielinsky, M. 1998, *A&A*, 336, 697
- Van Langevelde, H.J., Frail, D.A., Cordes, J.M. & Diamond, P.J. 1992, *ApJ*, 396, 686

- Vazquez-Semadeni, E. 1999, in the Proceedings of "The Chaotic Universe", Roma/Pescara, Italy, 1-5 Feb. 1999, eds. V. Gurzadyan and L. Bertone
- Vazquez-Semadeni, E., & Passot, T. 1999, Properties of Atomic Gas in Spiral Galaxies, in *Interstellar Turbulence*, eds. Jose Franco & Alberto Carraminana, p 223
- Wall, W.F., & Waller, W.H. 1998, in *New Horizons from Multi-Wavelength Sky Surveys*, eds. B.J. McLean et al., IAU 179, Kluwer, p. 191
- Waller, W.H., Varosi, F., Boulanger, F., & Digel, S.W. 1998, in *New Horizons from Multi-Wavelength Sky Surveys*, eds. B.J. McLean et al., IAU 179, Kluwer, p. 194
- Wilson, O.C., Munch, G., Flather, E.M., & Coffeen, M.F. 1959, *ApJS*, 4, 199
- Zurflueh, E.G. 2967, *Geophys.*, 32, 1015